

Neurons Limit Angiogenesis by Titrating VEGF in Retina

Keisuke Okabe,^{1,2,14} Sakiko Kobayashi,^{1,14} Toru Yamada,^{1,3} Toshihide Kurihara,⁴ Ikue Tai-Nagara,¹ Takeshi Miyamoto,⁵ Yoh-suke Mukouyama,⁷ Thomas N. Sato,^{8,9,10,11,12} Toshio Suda,⁶ Masatsugu Ema,¹³ and Yoshiaki Kubota^{1,*}

¹The Laboratory of Vascular Biology

²Department of Plastic Surgery

³Department of Surgery

⁴Department of Ophthalmology

⁵Department of Orthopedic Surgery

⁶Department of Cell Differentiation, The Sakaguchi Laboratory

School of Medicine, Keio University, 35 Shinanomachi, Shinjuku-ku, Tokyo 160-8582, Japan

⁷Laboratory of Stem Cell and Neuro-Vascular Biology, Genetics and Developmental Biology Center, National Heart, Lung, and Blood Institute, National Institutes of Health, Building 10/6C103, 10 Center Drive, Bethesda, MD 20892, USA

⁸ERATO Sato Live Bio-Forecasting Project, Japan Science and Technology Agency, Kyoto 619-0288, Japan

⁹Advanced Telecommunications Research Institute International, Kyoto 619-0288, Japan

¹⁰Department of Biomedical Engineering, Ithaca, NY 14850, USA

¹¹Graduate School of Biological Sciences, Nara Institute of Science and Technology, Nara 630-0192, Japan

¹²Centenary Institute, Sydney NSW 2050, Australia

¹³Research Center for Animal Life Science, Shiga University of Medical Science, Seta, Tsukinowa-cho, Otsu, Shiga 520-2192, Japan

¹⁴Co-first author

*Correspondence: ykubo33@a3.keio.jp

<http://dx.doi.org/10.1016/j.cell.2014.09.025>

SUMMARY

Vascular and nervous systems, two major networks in mammalian bodies, show a high degree of anatomical parallelism and functional crosstalk. During development, neurons guide and attract blood vessels, and consequently this parallelism is established. Here, we identified a noncanonical neurovascular interaction in eye development and disease. VEGFR2, a critical endothelial receptor for VEGF, was more abundantly expressed in retinal neurons than in endothelial cells, including endothelial tip cells. Genetic deletion of VEGFR2 in neurons caused misdirected angiogenesis toward neurons, resulting in abnormally increased vascular density around neurons. Further genetic experiments revealed that this misdirected angiogenesis was attributable to an excessive amount of VEGF protein around neurons caused by insufficient engulfment of VEGF by VEGFR2-deficient neurons. Moreover, absence of neuronal VEGFR2 caused misdirected regenerative angiogenesis in ischemic retinopathy. Thus, this study revealed neurovascular crosstalk and unprecedented cellular regulation of VEGF: retinal neurons titrate VEGF to limit neuronal vascularization.

INTRODUCTION

The vascular and nervous systems are two major networks that run throughout the bodies of mammals. They are highly interactive in both physiological (Mukouyama et al., 2002) and pathological (Lambrechts et al., 2003) settings and share some critical guidance molecules (Lu et al., 2004; Adams and Eichmann, 2010; Erskine et al., 2011).

The retina, a part of the central nervous system, is postnatally vascularized basically through sprouting angiogenesis (Dorrell et al., 2002; Gariano and Gardner, 2005; Pitulescu et al., 2010). During the first week of life in rodents, the retinal vasculature grows along the ganglion cell layer (GCL), the innermost surface of the retina forming the superficial vascular plexus, but does not grow into the area where neurons and neuronal progenitors exist (i.e., neuroretina). Afterward, the deep and intermediate vascular plexuses are serially formed, and three vascular plexuses are completed ~3 weeks after birth (Milde et al., 2013; Gerhardt et al., 2003; Gariano and Gardner, 2005). Within the GCL, astrocytes form a mesh before the vascular growth and guide angiogenic growth by providing vascular endothelial growth factor (VEGF) and extracellular matrices (Dorrell et al., 2002; Gerhardt et al., 2003; Ruhrberg et al., 2002; Stenzel et al., 2011). Therefore, it is conceivable that the astrocytic template holds the vasculature in the GCL and keeps it from growing into the neuroretina. However, pharmacological or genetic ablation of astrocytes does not cause abnormal growth of blood vessels into the neuroretina (Gerhardt et al., 2003; Fruttiger et al., 1996),

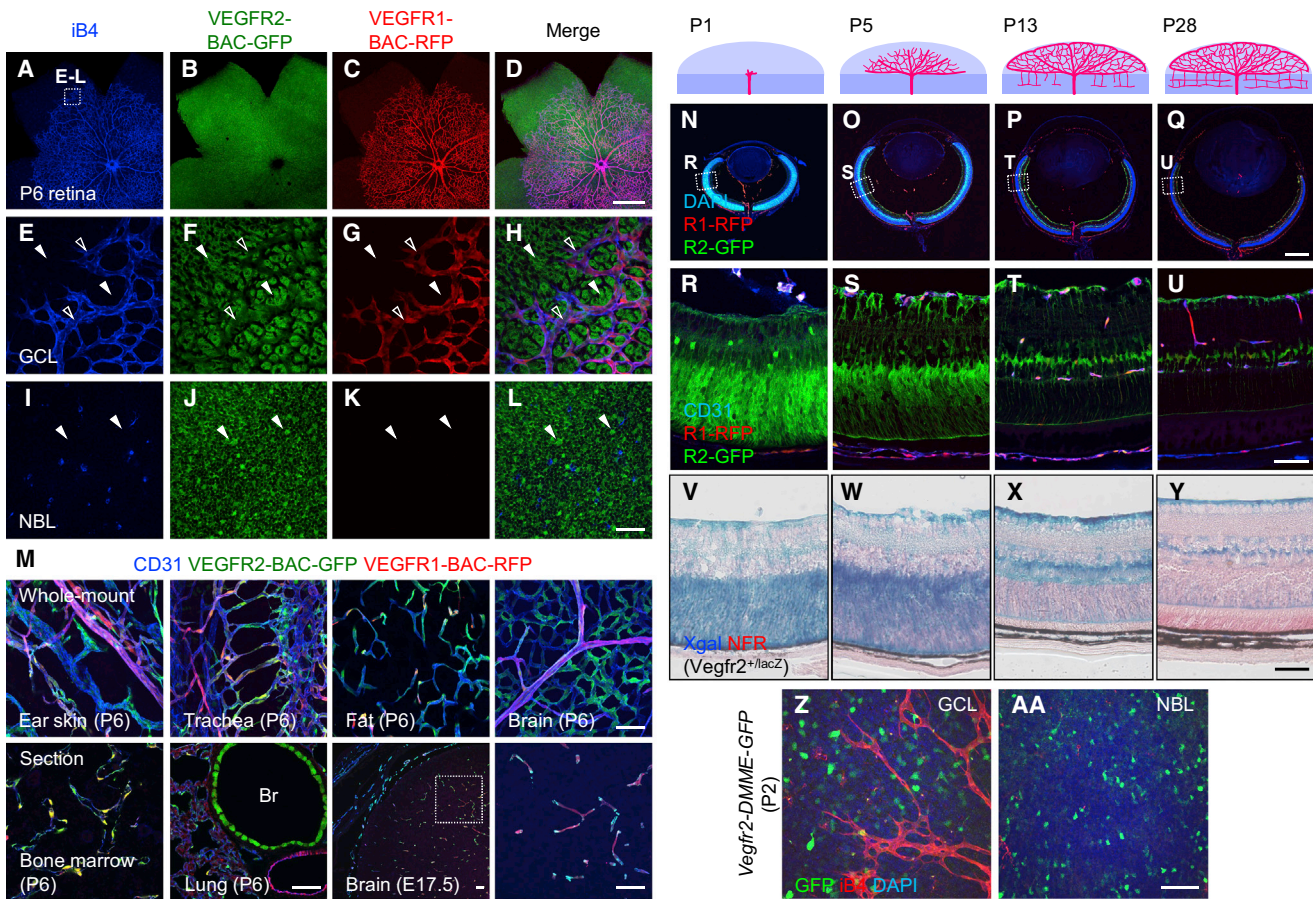


Figure 1. VEGFR2 Is More Highly Expressed in Retinal Neurons Than in Endothelial Cells

(A–M) Immunostaining of whole-mount tissues or sections from *Vegfr2-BAC-EGFP⁺Vegfr1-BAC-DsRed⁺* mice. In retina, GFP is more abundant in neurons (closed arrowheads) than in endothelial cells (open arrowheads). In ear skin, trachea, fat, brain, and bone marrow, GFP and RFP are restricted to endothelial cells, except for GFP expression in Clara cells of lung bronchioles (Br).

(N–Y) Immunohistochemistry in retinal sections from *Vegfr2-BAC-EGFP⁺Vegfr1-BAC-DsRed⁺* mice (N–U) and X-gal staining in the retina of *Vegfr2^{+/lacZ}* mice (V–Y) at various developmental stages. VEGFR2 is strongly expressed in neuroretina during the first postnatal week.

(Z and AA) Whole-mount staining for P2 retinas. Scale bars represent 500 μm (A–D and N–Q) and 50 μm (E–M and R–AA).

See also Figure S1.

suggesting the existence of some unknown cellular mechanism for neurovascular interaction. Here, we identified a noncanonical neurovascular interaction in eye development and disease; neurons titrate VEGF to determine the direction of angiogenesis, ensuring an appropriate level of vascular supply.

RESULTS

VEGFR2 Is More Abundant in Retinal Neurons Than in Endothelial Cells

Several reports have suggested that VEGFR2 is expressed in some neuronal cells in the retina (Yang and Cepko, 1996; Saint-Geniez et al., 2008; Kubota et al., 2011), but its details remain ambiguous. Therefore, we examined the expression of VEGFR2 and VEGFR1 in retinas using recently developed bacterial artificial chromosome (BAC)-transgenic mice (Ishitobi et al., 2010; Matsumoto et al., 2012). Although VEGFR1 was restricted to endothelial cells, VEGFR2 was abundantly expressed in the

neuroretina, even more strongly than in endothelial cells including tip cells (Gerhardt et al., 2003) that lead angiogenic outgrowth (Figures 1A–1L). VEGFR2 expression was undetected in both astrocytes and macrophages (Figures S1A–S1F available online). This expression pattern was consistent with that observed in *Vegfr2^{+/EGFP}* knockin mice (Ema et al., 2006), although fewer neuronal cells were labeled in those mice (Figures S1G–S1J). In other tissues, both VEGFR1 and VEGFR2 were expressed only in endothelial cells, except for the unexpected VEGFR2 expression in lung Clara cells (Figure 1M). In this regard, Bellon et al., (2010) showed slight VEGFR2 expression in brain neurons by immunohistochemistry. It is likely that the VEGFR2 expression in brain neurons is under the level we could detect in VEGFR2-BAC-EGFP mice. Sectioned specimens showed that VEGFR2 was abundant throughout the neuroretina during the first week after birth, but gradually decreased as postnatal (P) development continued (Figures 1N–1U). Costaining with various markers indicated that the minor population of

VEGFR2-positive cells at P13 was Müller cells (Figures S1K–S1N). This temporal transition of VEGFR2 expression in the neuroretina was similarly detected in *Vegfr2^{+/-LacZ}* knockin mice (Shalaby et al., 1997) (Figures 1V–1Y) as well as in the VEGFR2 immunohistochemical analysis (Figures S1O–S1R). Next, we explored the regulatory mechanism for the neuroretinal *Vegfr2* expression that diminishes after the neonatal period. We recently reported an enhancer of *Vegfr2*, the distal-multipotent-mesodermal-enhancer (DMME), which contains Gata-, Cdx-, Tcf/Lef-, ER71/Etv2-, and Fox-binding sites (Ishitobi et al., 2011). The DMME is active in hemangioblasts and cardiovascular progenitors, but not in endothelial cells. In the DMME-GFP reporter mice, the DMME was active in the neuroretina of neonates (Figures 1Z and 1AA) but not in stages after P7 (data not shown). Taken together, these data indicate that VEGFR2 is strongly expressed in the neuroretina when the neuronal area is avascular.

Misdirected Sprouting in Neuronal *Vegfr2* Knockout Mice

To determine the function of VEGFR2 in the neuroretina, we crossed *Vegfr2^{-flox}* mice with *Pax6 α -Cre* mice (Marquardt et al., 2001; Kurihara et al., 2010; Nakamura-Ishizu et al., 2012), which express Cre specifically in the neuroretina, apart from the area near the optic nerve head (Figures S2A and S2B). The resultant conditional knockout mice (*Pax6 α -Cre⁺Vegfr2^{flox/flox}*; *Vegfr2 ^{Δ neuro}* mice) showed ragged and caved edges in their vascular fronts, accompanied by persistent hyaloid vessels and a slight delay in the radial growth compared to that in control mice (*Pax6 α -Cre-Vegfr2^{flox/flox}*) (Figures 2A, 2E, and 2N). A striking abnormality was observed in the 3D direction of the vascular growth. At P6, *Vegfr2 ^{Δ neuro}* mice showed abundant vertical branching into the neuroblastic layer, and this was absent in control mice (Figures 2A–2N and S2C–S2F). These vertical branches in *Vegfr2 ^{Δ neuro}* mice had a normal morphology similar to that observed in VEGF-guided sprouting vessels utilizing tip cell filopodia (Gerhardt et al., 2003) (Figures 2H and 2K) and different from the pathologically aberrant invaginations observed in adult mice with a very low density lipoprotein receptor deficiency (Dorell et al., 2009). Comparable numbers of total endothelial cells quantified using fluorescence-activated cell sorting (FACS) analysis suggested that the defect in *Vegfr2 ^{Δ neuro}* mice is misdirected vascular growth rather than additional angiogenesis (Figure S2G). In a later stage at P9, when control mice had just started to form vertical branches, deep and intermediate plexuses were already formed in *Vegfr2 ^{Δ neuro}* mice (Figures 2O–2T). At P28, vessel branching in intermediate and deep plexuses was remarkably increased in *Vegfr2 ^{Δ neuro}* mice (Figure S2H–P). Deletion of *Vegfr2* in endothelial cells (*VEcad-Cre^{ERT2}+Vegfr2^{flox/lox}*; *Vegfr2 ^{Δ EC}*) severely impaired the radial vascular growth but did not lead to sprouting misdirected into the neuroretina (Figures 2U–2X). In addition, a myeloid-specific *Vegfr2* deletion (*Vav1-iCre⁺Vegfr2^{flox/lox}*; *Vegfr2 ^{Δ myeloid}*) using *Vav1-iCre* (de Boer et al., 2003) did not affect retinal vascularization (Figures S2Q–S2V).

Normal Retinogenesis in Neuronal *Vegfr2* Knockout Mice

VEGFR2 functions as a neurotrophic factor for brain neurons in pathologies such as amyotrophic lateral sclerosis (Lambrechts

et al., 2003). In addition, VEGFR2 is functional in adult retinal neurons (Saint-Geniez et al., 2008; Nishijima et al., 2007). Indeed, we detected phosphorylated VEGFR2 (pVEGFR2) proteins at P3 in the peripheral half of retinal tissues, which largely consist of neurons and completely lack vascular structure (Figure S3A). Considering these data, we hypothesized that the vascular phenotype in *Vegfr2 ^{Δ neuro}* mice is a secondary effect in degenerated retinal neurons. However, to our surprise, immunohistochemical analysis in the retinas of *Vegfr2 ^{Δ neuro}* mice indicated no detectable abnormalities in neuronal thickness, morphology, proliferation, or survival (Figures 3A–3I, 3N–3P, and S3B–S3L), suggesting that other neurotrophic factors masked the effect of VEGFR2 in vivo. Conversely, *Vegfr2 ^{Δ EC}* showed decreased retinal thickness, particularly in the thickness of the inner plexiform layer (IPL) (Figures S3C, S3F, S3I, S3K, and S3L), likely due to an insufficient vascular supply to the neuroretina. Transmission electron microscopy revealed that the vertical sprouts in *Vegfr2 ^{Δ neuro}* mice extended between normal ganglion cells (Figures 3J–3M). Retinal vascularization is guided by astrocytes (Gerhardt et al., 2003; Fruttiger et al., 1996) and ganglion cells (Sapieha et al., 2008; Binet et al., 2013). In *Vegfr2 ^{Δ neuro}* mice, the morphology of such guidance cells was not altered and the vertical branching proceeded below their mesh (Figures 3Q–3V). The electroretinography showed intact visual function of retinal neurons in *Vegfr2 ^{Δ neuro}* mice (Figures 3W and 3X). Immunostaining with cell-type-specific markers indicated the differentiation into all neuronal cell types was completed in adult *Vegfr2 ^{Δ neuro}* mice (Figure S3M).

Inadequate VEGF Endocytosis in Neuronal *Vegfr2* Knockout Mice

Next, we hypothesized that the expression of angiogenic or anti-angiogenic cytokines might be altered in *Vegfr2 ^{Δ neuro}* mice. However, quantitative PCR analysis failed to detect a significant difference in all of them between control and *Vegfr2 ^{Δ neuro}* mice (Figure 4A), and some of these results were confirmed using the analysis of their protein levels (Figure S4A). In the western blot analysis, we found the amount of VEGF-A protein was increased in the extracellular spaces of *Vegfr2 ^{Δ neuro}* mice (Figures 4B and 4C). VEGFR2 is actively endocytosed in endothelial cells, especially those cells located in vascular fronts (Nakayama et al., 2013; Lampugnani et al., 2006). Thus, this finding prompted us to test whether a similar event occurs in the neuroretina. Multiple VEGF-A-positive and early endosomal antigen 1 (EEA1)-positive spots were detected in neuroretinal cells (Figures 4D–4I). As was shown in endothelial cells, colocalization of endocytosed VEGF and VEGFR2 was detected in retinal neurons (Figures S4B–S4J). We also explored the fate of the internalized VEGF-A in neurons using an in vitro assay. Alexa 546-labeled hVEGF was administered into the culture of retinal neurons sorted using FACS (GFP⁺ cells from *Pax6 α Cre⁺flox-CAT-EGFP⁺* retinas). Endocytosis of the labeled VEGF occurred 10 min after administration, and VEGF⁺ endosomes were gradually decreased after removal of the labeled VEGF (Figures S4K–S4N). These data indicate that, as in endothelial cells (Lampugnani et al., 2006), endocytosed VEGF proteins are immediately degraded proteolytically and are not accumulated or recycled in retinal neurons. VEGF-A endocytosis in *Pax6 α -Cre⁺* cells in

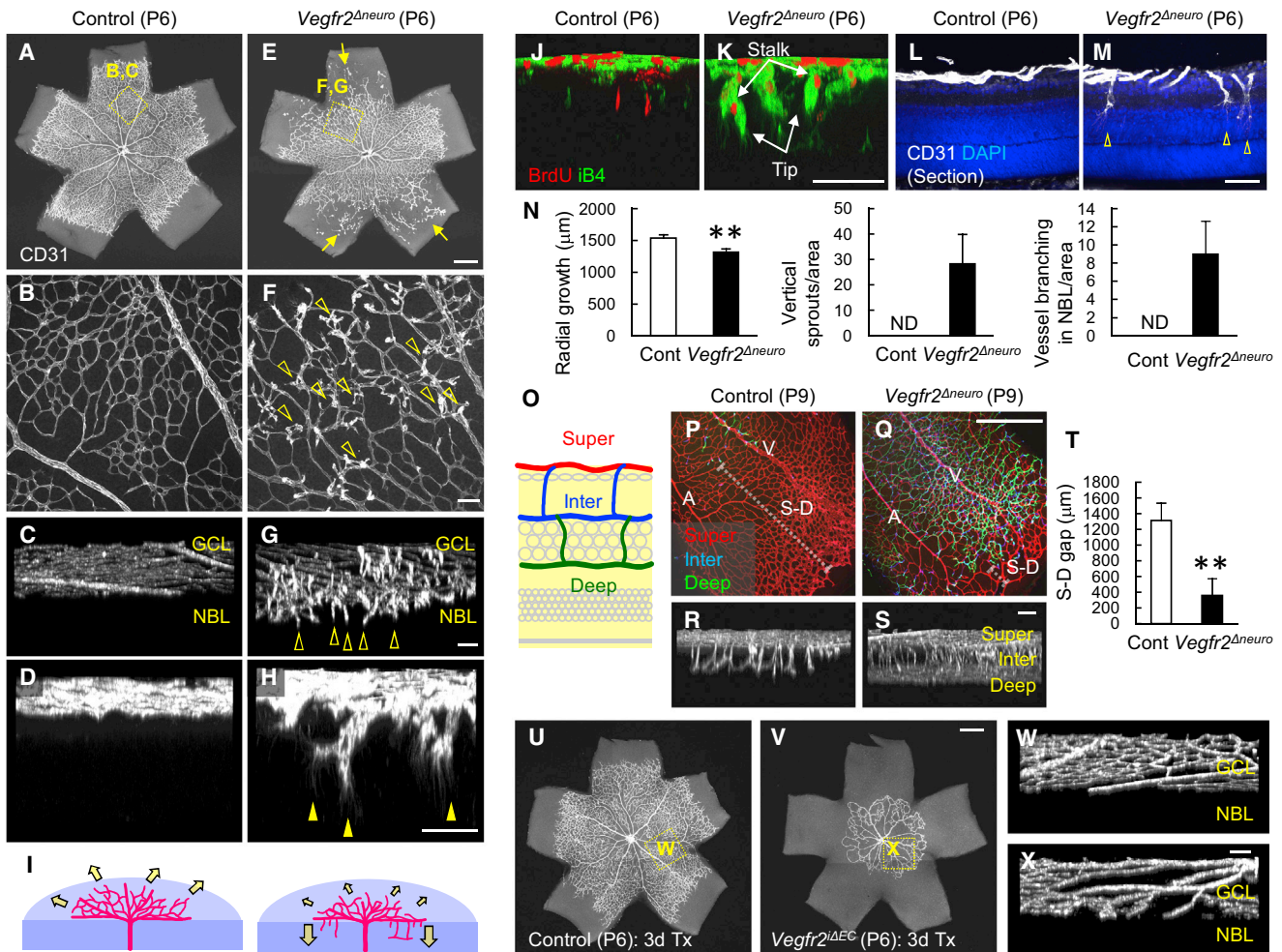


Figure 2. Misdirected Sprouting in Neuronal Vegfr2 Knockout

(A–H) Whole-mount staining in retina at P6. (C, D, G, and H) 3D images from multiple z stack scanning slices of the ganglion cell layer (GCL) to the neuroblastic layer (NBL). Caved edges and vertical branches (open arrowheads) with tip cell filopodia (closed arrowheads) as well as persisting hyaloid vessels (arrows) are observed in *Vegfr2^{Δneuro}* but not in control mice.

(I) Scheme depicting misdirected angiogenesis in *Vegfr2^{Δneuro}* mice.

(J–M) Immunostaining of whole-mount retinas (J and K) or thick sections (60 μm) (L and M) at P6. Vertical branches in *Vegfr2^{Δneuro}* mice growing into the neuroretina (open arrowheads).

(N) Quantification at P6 (n = 5).

(O) Scheme depicting three vascular plexuses in adult retinas.

(P–T) Whole-mount staining and quantification of retina at P6. The gap between the vascular front of superficial and deep plexuses (S–D gap: dotted line in P, Q) measured midline between arteries (A) and veins (V).

(U–X) Whole-mount staining of retina at P6. *Vegfr2^{ΔECC}* indicates the retina of *VEcad-Cre^{ERT2} + Vegfr2^{flx/flx}* mice treated with 4-hydroxytamoxifen (4OHT) for three days. Scale bars represent 500 μm (A, E, P, Q, U, and V); 50 μm (B–D, F–H, J–M, R, S, W, and X); **p < 0.01; ND, not detected. Data are represented as mean ± SD. See also Figure S2.

Vegfr2^{Δneuro} mice was almost undetectable (Figures 4J–4L). All of these data suggested that an excessive amount of VEGF-A protein in the neuroretinal layer caused preterm vertical growth of blood vessels. Previously, we reported that mice with a *Pax6α-Cre*-mediated *Vhl* deletion (*Vhl^{Δneuro}* mice) show a persistence of hyaloid vessels through insufficient suppression of the HIF1α/VEGF-A pathway (Kurihara et al., 2010). When we examined the retina of *Vhl^{Δneuro}* mice with VEGF-A expression levels more than four times higher than those of wild-type mice, we

found that *Vhl^{Δneuro}* mice exhibited early vertical branching from primary vascular plexuses (Figures 4M–4R). Normalization of VEGF-A levels by concomitant deletion of *Hif1α* abolished this misdirected branching (Figures 4S–4U).

Deletion of VEGF in Neurons Normalizes Neuronal Vegfr2 Knockout Mice

Based on the data above, we hypothesized that neuronal VEGFR2 spatiotemporally regulates the amount of VEGF-A

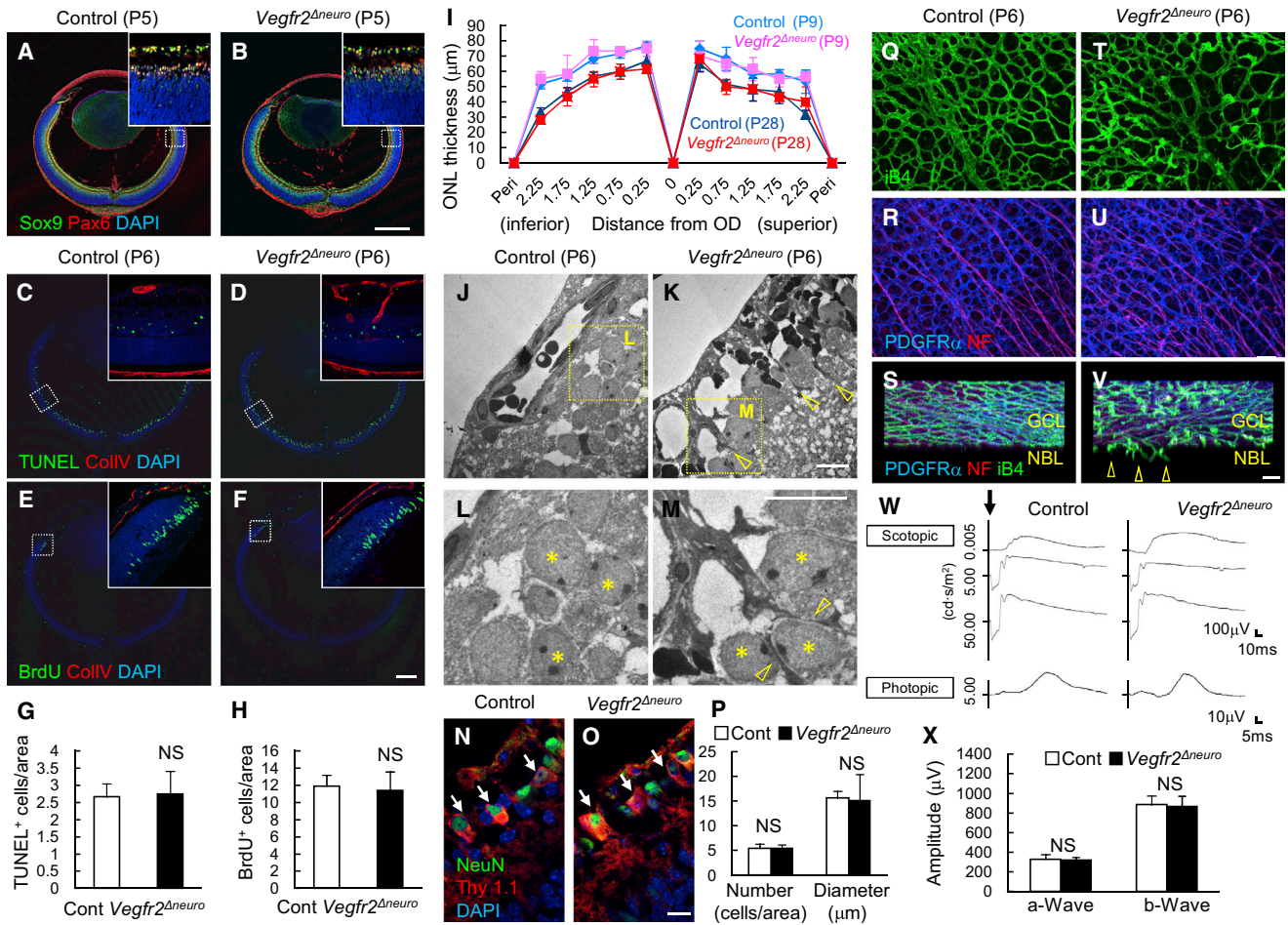


Figure 3. Normal Retinogenesis in Neuronal Vegfr2 Knockout

(A–F) Section staining of retinas at P5 (A and B) or P6 (C–F). Physiological apoptosis in the inner nuclear layer and proliferation in the most peripheral area are similarly detected in both control and *Vegfr2^{Δneuro}* mice.

(G and H) Quantification at P6 (n = 4).

(I) Retinal thickness quantified at various distances from the optic disk (OD) at P9 or P28.

(J–M) Transmission electron microscopy of retina at P6. Vertical sprouting (arrowheads) between normal ganglion cell bodies (asterisks).

(N and O) Staining of retinal sections at P6. Arrows indicate retinal ganglion cells.

(P) Quantification of double-labeled NeuN⁺Thy1.1⁺ ganglion cells at P6 (n = 5).

(Q–V) Whole-mount staining of retina at P6. Vertical sprouts in *Vegfr2^{Δneuro}* mice are projected below the mesh of astrocytes and neurofilaments (open arrowheads).

(W and X) Electrorretinography at P28. Representative wave responses (W) and amplitude quantification of a-waves and b-waves (X) (n = 4). Scale bars represent 500 μm (A–F); 50 μm (Q–V); 10 μm (J–O); NS, not significant. Data are represented as mean ± SD.

See also Figure S3.

protein near neurons and consequently orchestrates the timing of vertical branching into deep retinal layers. To test this hypothesis, we pharmacologically decreased the amount of VEGF-A with intraocular injections of Flt1/Fc chimeric proteins that bind and inactivate VEGF proteins (Kurihara et al., 2010). Although injections of more than 500 ng of Flt1/Fc proteins impaired the radial growth of superficial plexuses (data not shown), injections of 50 ng did not significantly affect the superficial plexus but normalized the vertical branching in *Vegfr2^{Δneuro}* mice (Figures 5A–5I and 5V). We confirmed this finding genetically by generating mice with *Pax6α-Cre*-mediated simultaneous deletions of *Vegfa* and *Vegfr2* because VEGF-A is expressed in retinal neu-

rons as well as astrocytes (Figures S5A and S5B) in accordance with a previous report (Saint-Geniez et al., 2008). Double knockout mice (*Pax6α-Cre⁺Vegfr2^{fllox/fllox}Vegfa^{fllox/fllox}*) did not show the early vertical branching observed in *Vegfr2^{Δneuro}* mice (Figures 5J–5U and 5W). Consistent with the data generated in the *Nestin-Cre*-mediated *Vegfa* deletion (Haigh et al., 2003), the *Pax6α-Cre*-mediated *Vegfa* deletion did not disturb the overall vascular architecture of superficial vascular plexuses, except for some arteriovenous crossings (Figure 5O), as was also seen in double knockout mice (Figure 5Q). We performed VEGF immunohistochemistry on retinal sections of mutant mice to determine the spatial distribution of VEGF. Consistent

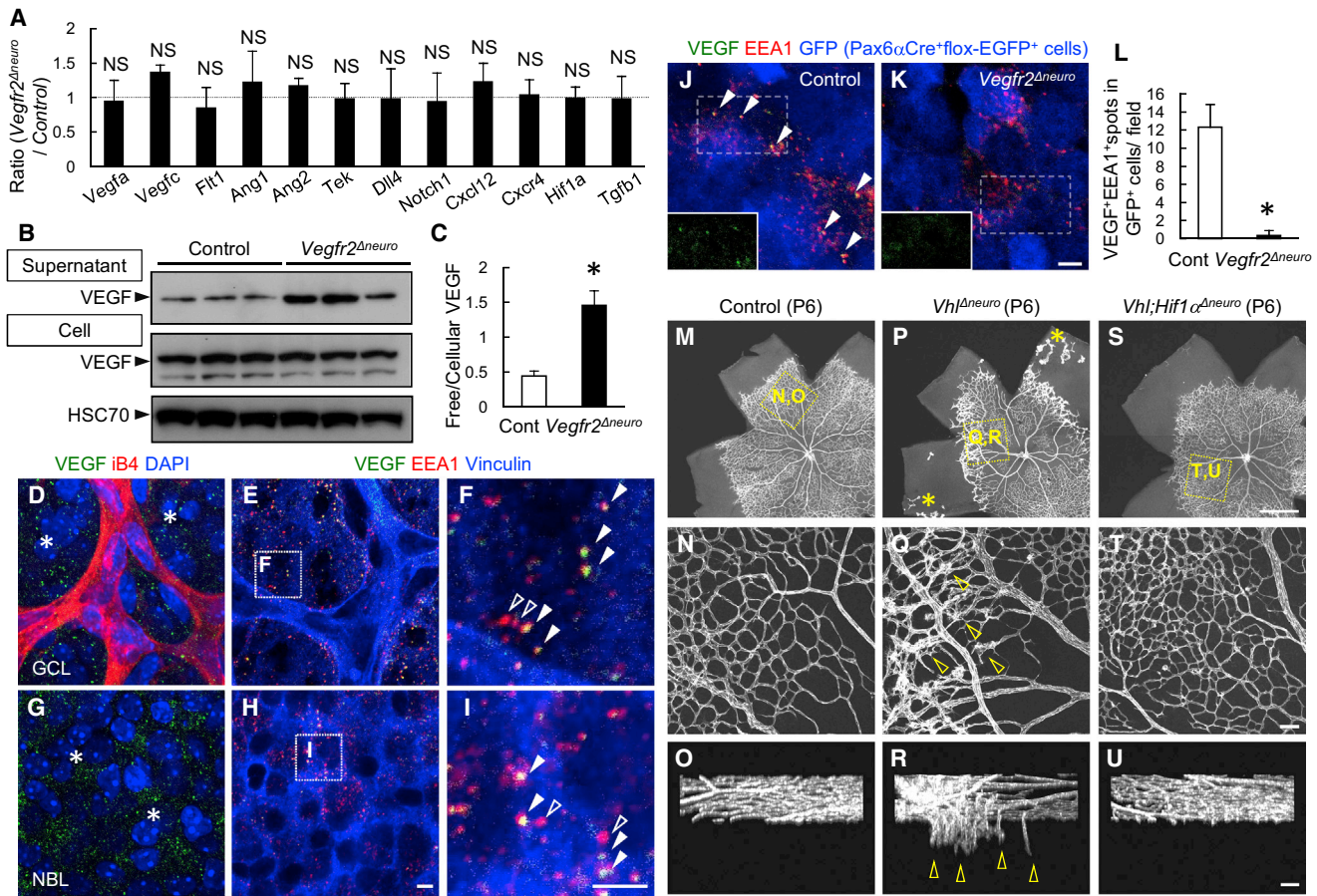


Figure 4. Insufficient VEGF Endocytosis in Neuronal Vegfr2 Knockout

(A) Quantitative PCR analysis of angiogenic factors in retinal tissues at P6 (n = 4).

(B and C) Western blot analysis and quantification of relative intensity (n = 3) for supernatant and cellular components separated by enzymatic dissociation and centrifugation.

(D–L) Whole-mount staining and quantification for P6 retinas (10 fields (50 μm × 50 μm) averaged in each of three individuals). VEGF-A-positive spots detected in the cytoplasm of retinal neurons (asterisks). Some EEA1-positive early endosomes contain VEGF-A (closed arrowheads) but others do not (open arrowheads). Insets in (J) and (K) show only green channels in the grid areas.

(M–U) Whole-mount staining for P6 retinas. Not only persisting hyaloid vessels (asterisks) but also early vertical branches (arrowheads) are detected in *Vhl*^{Δneuro} but not in control and *Vhl*; *Hif1α*^{Δneuro} mice. Scale bars represent 500 μm (M, P, and S); 50 μm (N, O, Q, R, T, and U); 5 μm (D–K); *p < 0.05; NS, not significant; ND, not detected. Data are represented as mean ± SD.

See also Figure S4.

with the idea of local VEGF sequestering by VEGFR2-positive neurons, VEGF immunoreactivity was strongly detected in the neuroretina of *Vegfr2*^{Δneuro} and *Vhl*^{Δneuro} and was normalized or rather decreased in *Vhl*; *Hif1α*^{Δneuro} and *Vegfr2*; *Vegfa*^{Δneuro} (Figures S5C–S5J).

Endocytosis Deficiency Recapitulates Defects in Neuronal Vegfr2 Knockout Mice

The above data indicated that misdirected angiogenesis was caused by excessive VEGF protein around the neurons of *Vegfr2*^{Δneuro} mice, which was likely due to insufficient endocytosis of VEGF. However, another possible explanation is the lack of soluble Vegfr2 (sVegfr2), a splice variant of the gene encoding Vegfr2 that encodes a secreted form of the protein (Albuquerque et al., 2009). Theoretically, the lack of the VEGF

sequestering ability by sVegfr2 could increase free VEGF proteins, resulting in premature vascular invasion, as seen in *Vegfr2*^{Δneuro} mice. In an RT-PCR analysis of various tissues, we found that sVegfr2 expression was relatively abundant in retinal tissues (Figures S6A and S6B). To functionally evaluate sVegfr2 in the retina, we generated mice lacking sVegfr2 but not membrane bound Vegfr2 (mbVegfr2) by deleting intron13, which is responsible for this splice variant (Figures 6A and 6B). Analysis of the neonatal skin clearly indicate lymphatic vessels are apparently enlarged and hyperplastic in mice with the systemic deletion of sVegfr2 (*Vegfr2*^{Δs/Δs}) (Figures S6C and S6D) in agreement with a previous paper (Albuquerque et al., 2009). However, *Vegfr2*^{Δs/Δs} and mice with the neuron-specific deletion of sVegfr2 (*Pax6α*-*Cre*⁺*Vegfr2*^{fllox/Δs}; *sVegfr2*^{Δneuro}) showed no misdirected retinal angiogenesis (Figures 6C–6K). Regarding

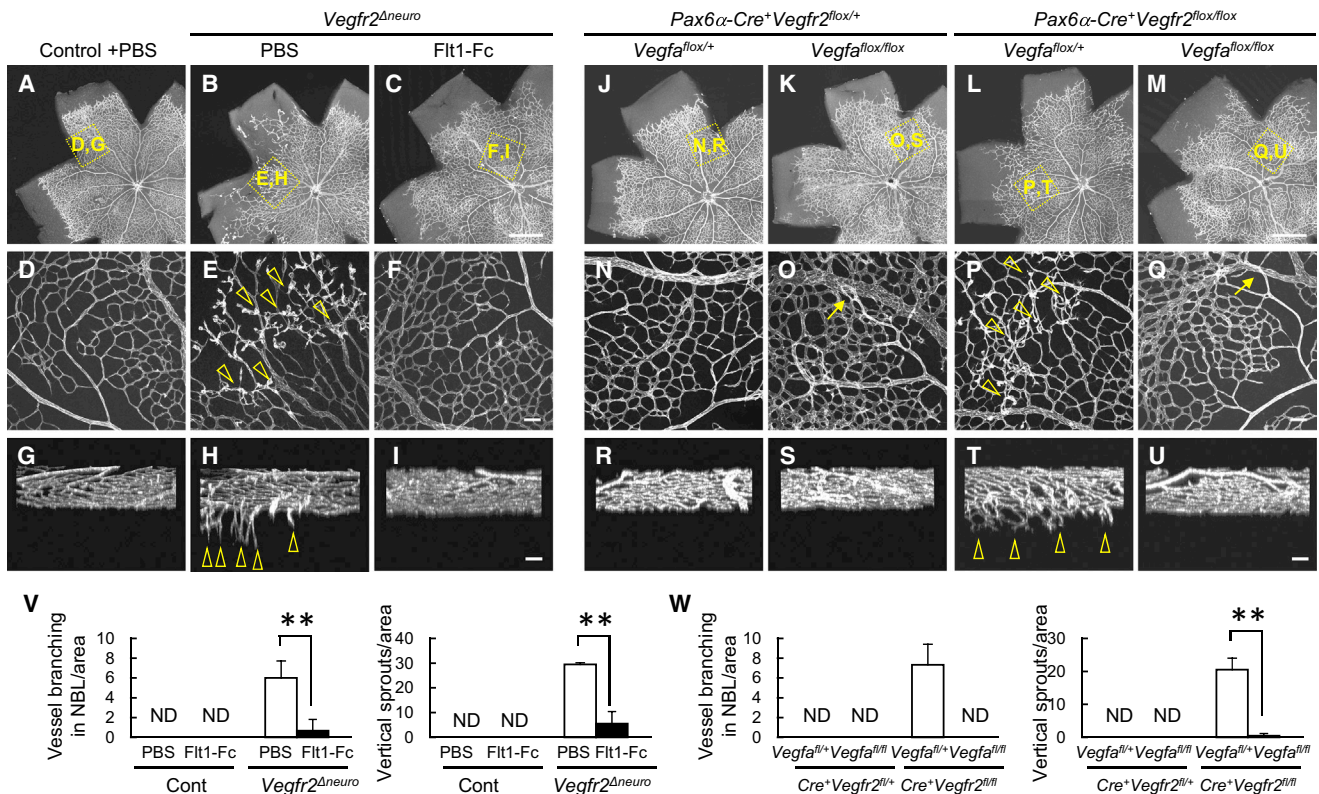


Figure 5. Reduction of VEGF-A Normalizes Neuronal Vegfr2 Knockout

(A–U) Whole-mount staining of retina at P6 and quantification (n = 4). Vertical branches (arrowheads) seen in *Vegfr2^{Δneuro}* mice are abolished by intraocular injection of Flt1/Fc chimeric proteins at P4 or neuronal Vegfa deletion. Arrows in (O) and (Q) indicate arteriovenous crossing. Scale bars represent 500 μm (A–C and J–M); 50 μm (D–I and N–U); **p < 0.01; ND, not detected. Data are represented as mean ± SD. See also Figure S5.

the lack of retinal phenotypes in *Vegfr2^{Δs/Δs}* and *sVegfr2^{Δneuro}*, a likely explanation is that the amount of sVegfr2 is very low, and thus its VEGF sequestering effect is negligible in retinal neurons. To clarify the involvement of endocytosis in retinal neurons, we conditionally deleted *Dynamin1* and *Dynamin2*, genes known to critically and cooperatively act on cellular endocytosis (Ferguson et al., 2009). In the retina of the resultant mutant mice (*Pax6α-Cre⁺Dnm1^{fllox/fllox}Dnm2^{fllox/fllox}; Dnm1;Dnm2^{Δneuro}*), early vertical sprouting occurred as expected, although the superficial plexus in these mice was more severely impaired than that in *Vegfr2^{Δneuro}* mice (Figures 6L–6Q). The morphology of the neuroretina was largely normal, but we detected insufficient separation of the inner nuclear layer (INL) and the outer nuclear layer (ONL) and reduced numbers of Pax6-positive cells in *Dnm1;Dnm2^{Δneuro}* mice (Figures S6E–S6J). In this regard, the phenotype in *Dnm1;Dnm2^{Δneuro}* mice might be attributable to angiogenic factors other than VEGF, such as Netrin1, Sema3A, and Sema3E, which are known to be expressed in retinal neurons and are involved in angiogenesis. To rule out this possibility, we performed a combinatorial deletion of VEGF on Dnm1 and Dnm2 knockouts, generating triple conditional knockout mice for these three genes in retinal neurons (*Pax6αCre⁺Dnm1^{fllox/fllox}Dnm2^{fllox/fllox}Vegfa^{fllox/fllox}; Dnm1;Dnm2;Vegfa^{Δneuro}*). We found that this mutant mouse showed no misdirected angiogenesis,

although the vascular defects in the superficial plexus remained similar to those in *Dnm1;Dnm2^{Δneuro}* mice (Figures 6N, 6Q, 6T, and 6U). In agreement with this result, the ratio of free to cellular VEGF proteins was increased in *Dnm1;Dnm2^{Δneuro}* mice, with no change in the transcription level (Figures 6V and 6W), as was observed in *Vegfr2^{Δneuro}* mice. These data indicate that other angiogenic factors or neuronal defects may be relevant to abnormalities in superficial plexuses, but premature vessel invasion is attributable to VEGF.

Misdirected Regenerative Angiogenesis in Neuronal Vegfr2 Knockouts in Retinal Pathology

Finally, we explored the effect of neuronal Vegfr2 deletion in pathological and regenerative angiogenesis in the ischemic retinopathy (Smith et al., 1994). Although the extent of pathological angiogenesis was not altered, regenerative angiogenesis into the vaso-obiterated area was decreased in *Vegfr2^{Δneuro}* mice (Figures 7A–7H). Looking closer at the leading edge, we found that *Vegfr2^{Δneuro}* mice showed abnormal vessels growing into intracapillary spaces (Figure 7D), likely the cause of delayed vascular regeneration. The reparative angiogenesis did not progress to the deep layer in either control or *Vegfr2^{Δneuro}* mice (Figures 7E and 7F). VEGFR2-positive neurons were markedly multilayered in the intracapillary spaces of the ganglion cell layer rather than

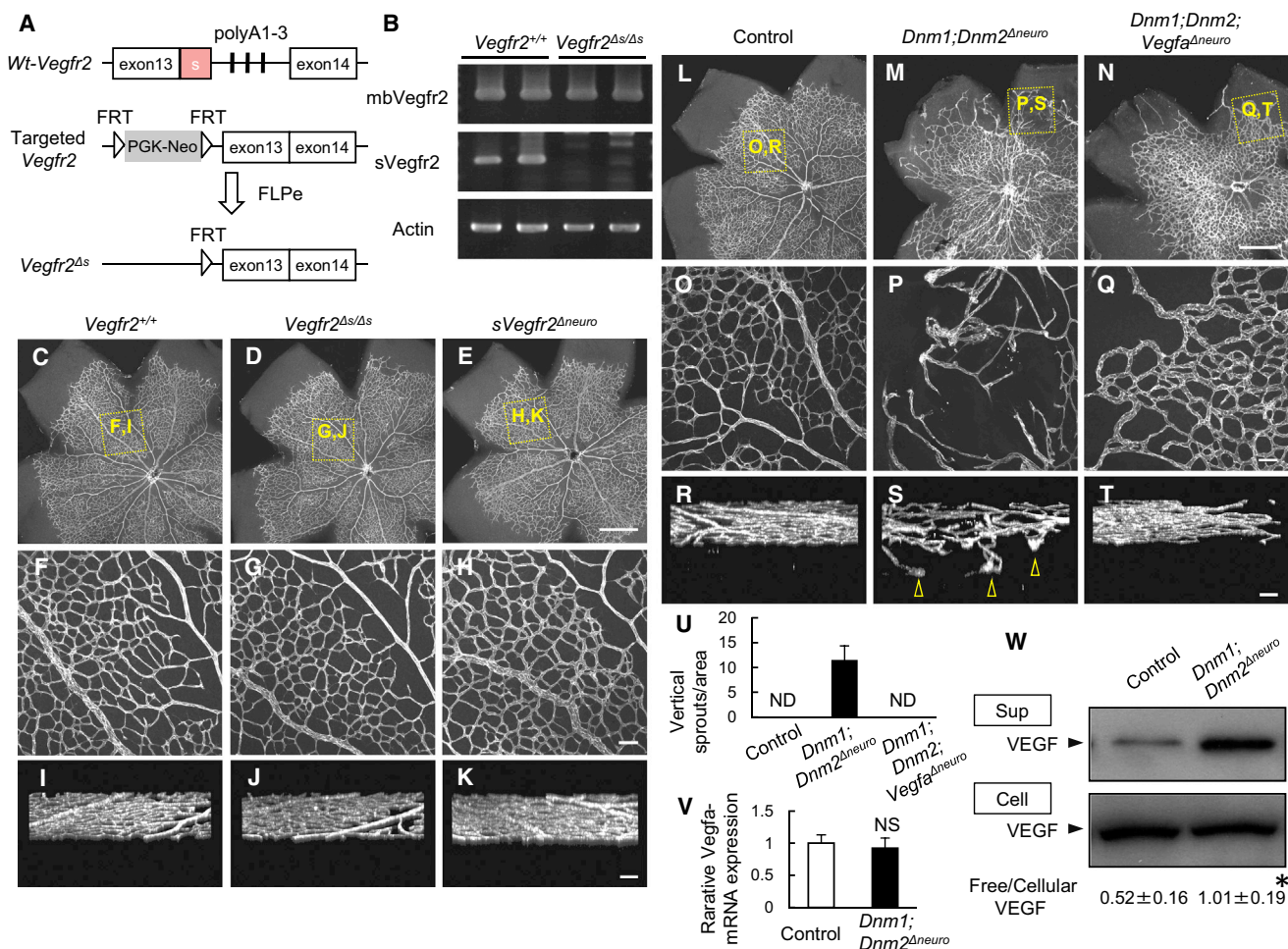


Figure 6. Significance of Endocytosis, but Not sVegfr2, in Misdirected Angiogenesis

(A) Scheme depicting the gene-targeting strategy for *Vegfr2^{Δs}*.

(B) RT-PCR analysis for P4 retinas. *Vegfr2^{Δs/Δs}* mice lack soluble Vegfr2 (*sVegfr2*) but not membrane bound Vegfr2 (*mbVegfr2*).

(C–T) Whole-mount staining for P6 retinas. Vertical branches are observed in *Dnm1;Dnm2^{Δneuro}* (arrowheads in S but not in *Dnm1;Dnm2;Vegfa^{Δneuro}* and mice lacking *sVegfr2*).

(U) Quantification at P6 (n = 4).

(V) Quantitative PCR analysis of *Vegfa* at P6 (n = 4).

(W) Western blot analysis and quantification of relative intensity at P6 (n = 3). Scale bars represent 500 μm (C–E and L–N); 50 μm (F–K and O–T); *p < 0.05; NS, not significant; ND, not detected. Data are represented as mean ± SD.

See also Figure S6.

in the deep layer (Figures 7I–7K). This feature was not observed in the normal physiological development occurring around this stage (Figures 1T and 1X). All of these expression data indicate that neuronal control of the amount of VEGF proteins in this disease model primarily functions in the horizontal retinal layer. The vaso-obiterated area immediately after hyperoxygen exposure showed no significant difference between control and *Vegfr2^{Δneuro}* mice (Figures 7L–7N).

DISCUSSION

In the developing retina, angiogenic growth led by VEGFR2⁺ endothelial tip and stalk cells proceeds according to the gradient

of VEGF mainly secreted by astrocytes (Gerhardt et al., 2003; Potente et al., 2011). Our results demonstrated that retinal neurons also highly expressed VEGFR2, thus binding and engulfing VEGF proteins around neurons. In neuron-specific deletions of *Vegfr2*, free VEGF proteins are markedly increased due to neurons insufficiently engulfing VEGF, which resulted in misdirected angiogenic growth toward neurons (Figure 7O).

Cell-autonomous VEGF signaling in endothelial cells is required for vascular homeostasis (Lee et al., 2007). In endothelial cells, intracrine VEGF binds internalized VEGFR2, and all the ligand-receptor actions take place in the cytoplasm. The auto-crine systems in the endothelium and neurons may differ slightly. Based on our data, it is likely that the VEGF produced by retinal

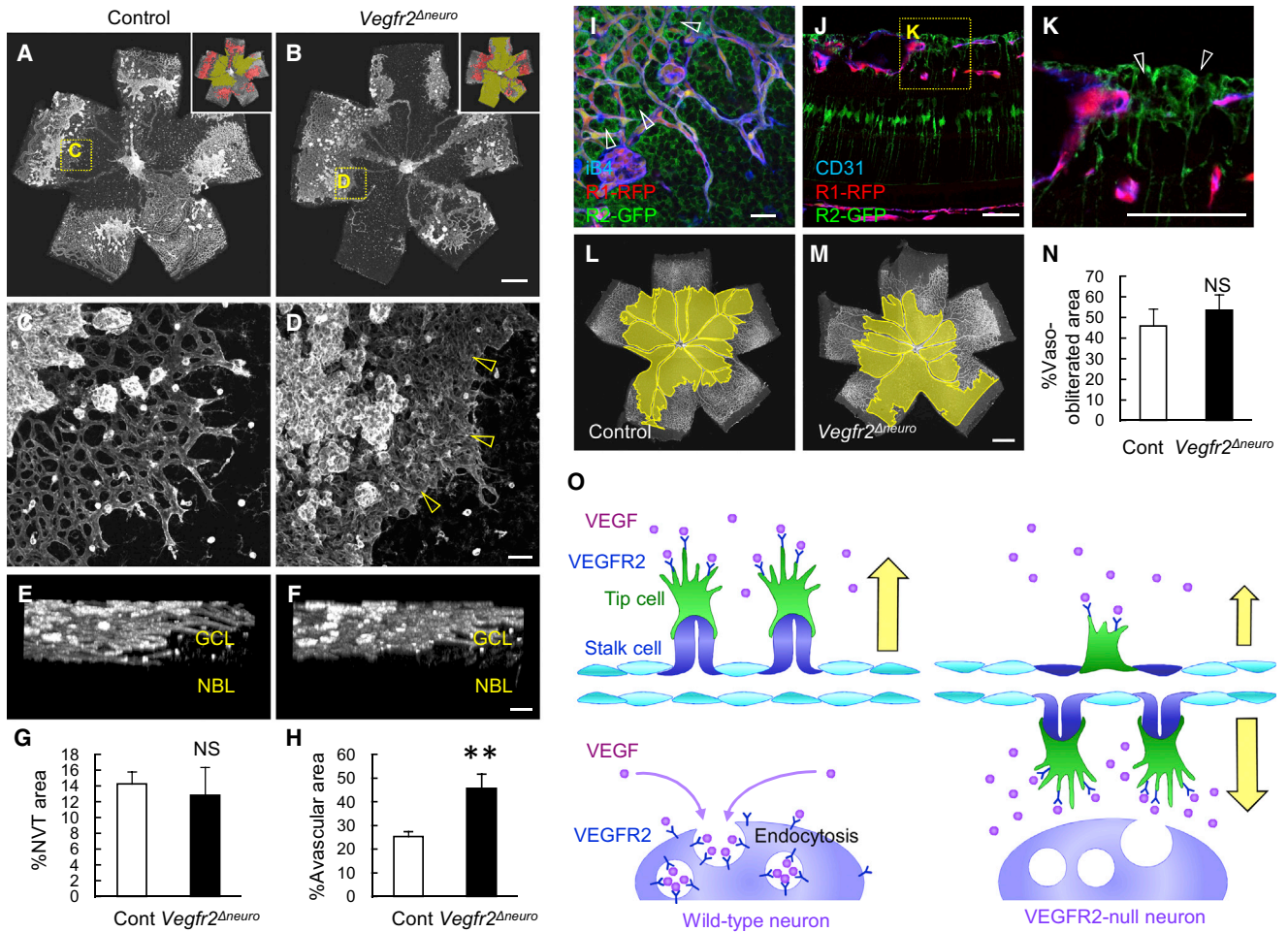


Figure 7. Misdirected Reparative Angiogenesis in Neuronal *Vegfr2* Knockout in Ischemic Retinopathy

(A–H) Whole-mount staining and quantification (n = 6) for P15 retinas with ischemic retinopathy. Abnormally growing vessels fill intravascular spaces in the leading edges of *Vegfr2^{Δneuro}* mice (arrowheads).

(I–K) Whole-mount tissues or sections of retinas at P15 with ischemic retinopathy from *Vegfr2-BAC-EGFP⁺Vegfr1-BAC-DsRed⁺* mice. VEGFR2-positive neurons are multilayered in the intracapillary spaces of the ganglion cell layer (arrowheads) rather than in the deep layer.

(L–N) Whole-mount staining and quantification (n = 4) for retinas with ischemic retinopathy at P11. Vaso-obiterated area (yellow) just after hyperoxygen exposure shows no significant difference between control and *Vegfr2^{Δneuro}* mice.

(O) Scheme depicting the angiogenic direction in the existence or absence of VEGFR2 in neurons. Normally, angiogenic growth led by VEGFR2⁺ endothelial tip and stalk cells proceeds according to the gradient of VEGF secreted by astrocytes, while neurons bind and engulf VEGF proteins around them. In the absence of neuronal VEGFR2, free VEGF proteins markedly increased due to insufficient endocytosis of VEGF, resulting in misdirected angiogenic growth toward neurons. Scale bars represent 500 μm in (A, B, L, and M); 50 μm in (C–F and I–K); **p < 0.01; NS, not significant. Data are represented as mean ± SD.

neurons is, if not all, secreted because the *Nestin-Cre-* (Haigh et al., 2003) or *Pax6α-Cre-* mediated deletion of *Vegfa* affects vascularization.

Stefater et al. (2011) recently reported that the loss of the Wnt/*Vegfr1* signaling in myeloid cells leads to an overgrowth of deep vascular plexus but not to early vertical sprouting. It is supposed that neurons and myeloid cells serially and cooperatively regulate the formation of the deep vascular plexus. Interesting vascular phenotypes are observed in mice lacking *Norrin*, which activates the canonical Wnt signaling via the endothelial *Frizzled4/LRP5* pathway. *Norrin* null mice show aberrant proliferation in vertical branches, which fail to extend to the inner nuclear layer, likely due to an enhanced response to antiangiogenic fac-

tors, such as class 3 semaphorins (Ye et al., 2009; Wang et al., 2012). Cooperation between VEGF/VEGFR2 and the *Norrin/Wnt* signaling may balance the timing and amount of vertical branching. One question is why the vertical vascular growth in *Vegfr2^{Δneuro}* mice stopped in the inner nuclear layer and did not grow into the outer nuclear layer. This may be explained by soluble VEGFR1 that binds VEGF proteins in photoreceptor layers (Luo et al., 2013).

During the first postnatal week, neuroretinal cells remain undifferentiated as retinal progenitor cells and postmitotic progenitors (Marquardt et al., 2001). We showed that DMME is active in these cells. Because DMME contains *Gata-*, *Cdx-*, *Tcf/Lef-*, *ER71/Etv2-*, and *Fox-* binding sites, neuroretinal *Vegfr2* expression is

likely under the control of the Wnt, Fgf, and Bmp families known to control the undifferentiated status of retinal progenitor cells (Lillien and Cepko, 1992; Kubo et al., 2005). A low oxygen environment, called a hypoxic niche, is suitable for maintaining stem cells (Mohyeldin et al., 2010), suggesting the compelling hypothesis that stem cell factors simultaneously contribute to creating a hypoxic niche via neuronal VEGFR2 expression as a tissue-specific mechanism.

One of the important issues we could not uncover is the biological significance of such a spill-over production of VEGF by neurons. We speculate that neuronal VEGF contributes to maintenance of hyaloid vessels (Lang, 1997), a part of the fetal-type circulatory system in retina. In embryonic retinas and the peripheral part of neonatal retinas, astrocytes are totally absent and neurons are the only source of VEGF. For maintenance of hyaloid vessels, neurons once excessively secrete VEGF proteins and then engulf them around neurons themselves. Supporting this idea, we previously showed that the overproduction of VEGF in neurons leads to persistence of hyaloid vessels (Kurihara et al., 2010). Moreover, our preliminary data using Dkk3-BAC-Cre, another retinal neuron-specific Cre line, indicate the complete deletion of VEGF in neurons ablates hyaloid vessels (data not shown).

Finally, the results of the present study revealed neurovascular crosstalk that explains how the retinal vascularization primarily radiates 2D along the GCL while the neuroretinal area remains avascular. Further analysis is expected to offer novel insights into the pathology of human retinal neovascular diseases, such as age-related macular degeneration and diabetic retinopathy, in which retinal neurovascular crosstalk is expected to be highly relevant.

EXPERIMENTAL PROCEDURES

Mice and Analysis

Animal care was performed in accordance with the Guidelines of Keio University for Animal and Recombinant DNA experiments. *Pax6 α -Cre* mice (Marquardt et al., 2001) were a gift from Peter Gruss (Max-Planck-Institute of Biophysical Chemistry). *Vegfr2^{Δ5/Δ5}* knockin mice and transgenic mice expressing Cre^{ERT2} under the control of the 200.3 kb VE-cadherin promoter sequence obtained from a BAC clone (RP23-453P1) were newly generated. The 4-hydroxytamoxifen (40 μ g) was subcutaneously injected at P3, P4, and P5. *Vegfa-flox* mice (Gerber et al., 1999) were kindly provided by Genentech. *Vhl-flox* (Haase et al., 2001) and *Hif1 α -flox* mice (Ryan et al., 2000) were gifts from Rudolf Jaenisch (The Whitehead Institute for Biomedical Research) and Randall Johnson (University of Cambridge), respectively. *Pax6 α -Cre* mice were mated with *Vegfr2-flox* mice (Hooper et al., 2009) to obtain neuron-specific *Vegfr2* knockout mice. *Vav1-iCre*, *Dnm1-flox* and *Dnm2-flox* mice were obtained from the Jackson Laboratory. Heterozygous pups of *Vegfr2^{+lacZ}* (Shalaby et al., 1997), *Vegfr1-BAC-DsRed*, *Vegfr2-BAC-EGFP*, and *Vegfr2-DMME-EGFP* (Ishitobi et al., 2011) mice were used. All mice were maintained on a C57BL/6J background.

Preparation of Whole-Mount Retinas

Eucleated eyes were fixed for 20 min in 4% paraformaldehyde (PFA) in PBS and then dissected. Retinal cups were postfixed for 30 min and then stained as described below.

Preparation of Retinal Sections

Eucleated eyes were fixed for 10 min in 4% PFA in PBS and then hemispheres were cut. After overnight postfixation, samples were snap-frozen in OCT compound (Sakura Finetechnical). All specimens were sectioned (10–60 μ m thick) at the plane of the optic disk.

Retinal Immunostaining and In Situ Hybridization

Immunohistochemistry (IHC) of whole-mount samples or tissue sections was performed as previously described (Kubota et al., 2011). For the BrdU incorporation assay, 100 μ g of BrdU per gram of body weight (BD Pharmingen) dissolved in sterile PBS was injected intraperitoneally 2 hr before sacrifice. Isolated retinas were stained using a BrdU immunohistochemistry kit (Calbiochem). The primary monoclonal antibodies used were hamster anti-CD31 (2H8; Chemicon), PDGFR α (APA5; eBioscience), neurofilament (2H3; Developmental Studies Hybridoma Bank), Pax-6 (Developmental Studies Hybridoma Bank), glutamine synthetase (BD Biosciences), F4/80 (Cl:A3-1; Serotech), GFAP (G-A-5; Cy3-conjugated; Sigma-Aldrich), Thy1.1 (Chemicon), Calbindin (Chemicon), PKC α (BD Transduction Laboratories), VEGFR2 (BD Pharmingen), and syntaxin (SP7; Millipore). The primary polyclonal antibodies used were anti-GFP (Alexa488-conjugated; Molecular Probes), rhodopsin (LSL), sox9 (Millipore), VEGF (Santa Cruz), LYVE-1 (RELIATech), NeuN (Abcam), and EEA1 (Sigma-Aldrich). Secondary antibodies used were Alexa 488 fluorescence-conjugated IgGs (Molecular Probes) or Cy3/Cy5 DyLight549/Dye-Light649-conjugated IgGs (Jackson ImmunoResearch). For nuclear staining, specimens were treated with DAPI (Molecular Probes). In some experiments, blood vessels and monocyte-lineage cells were simultaneously visualized using biotinylated isolectin B4 (Sigma) followed by fluorescent streptavidin conjugates (Molecular Probes). For in situ hybridization, retinas were briefly digested with proteinase K and hybridized with digoxigenin (DIG)-labeled antisense RNA probes, as described previously (Kubota et al., 2011). ImageJ software equipped with the colocalization plugin Coloc2 (NIH) was used to quantify colocalization events.

X-Gal Staining of Tissue Sections

Eucleated eyes were fixed for 10 min in 1% glutaraldehyde in PBS and then hemispheres were cut. After overnight postfixation, samples were snap-frozen in OCT compound (Sakura Finetechnical). Specimens were sectioned (10 μ m thick) at the plane of the optic disk. Tissue sections were incubated for 1 hr at 37°C with 1 mg/ml of X-gal in a standard X-gal reaction buffer (35 mM potassium ferrocyanide, 35 mM potassium ferricyanide, 2 mM MgCl₂, 0.02% NP-40, and 0.01% sodium deoxycholate in PBS).

Confocal Microscopy

Fluorescent images were obtained using a confocal laser scanning microscope (FV1000; Olympus). Quantification of cells or substances of interest was conducted on eight 500 μ m \times 500 μ m fields of view per sample in scanned images, and numbers obtained from each of the eight fields were averaged. To construct 3D images, multiple slices horizontally imaged from the same field of view at 0.5 μ m intervals were integrated using an FV10-ASW Viewer (Olympus).

Intraocular Injections

Injections into the vitreous body were performed using 33 gauge needles as described previously (Kubota et al., 2011). Sterile PBS (0.5 μ l) with or without 0.1 mg/ml of Flt1-Fc chimera proteins (R&D Systems) was injected at P4.

Ischemic Retinopathy Model

P8 mice with nursing mothers were maintained for 3 days in 85% oxygen and then placed back in room air in a modification of the previously described oxygen-induced retinopathy (OIR) model (Smith et al., 1994). ImageJ Software was used for the quantification of indicated areas in scanned images as previously described (Kubota et al., 2011).

Western Blotting

Western blot analysis was performed as described elsewhere (Kubota et al., 2011). The primary antibodies used were anti-VEGF (Santa Cruz), phosphorylated-VEGFR2 (Millipore), VEGFR2 (Cell Signaling), VEGF-C (RELIATech), Angiopoietin-1 (Santa Cruz), Angiopoietin-2 (Abcam), HIF1 α (Santa Cruz), HIF2 α (Abcam), and HSC70 (Santa Cruz). ImageJ software was used to measure the density of each band. For separation of extracellular and cellular components, retinal tissues were incubated for 30 min at 37°C in Dulbecco's minimum essential medium (DMEM) containing 1% collagenase D (from *Clostridium histolyticum*) before cells were dissociated by gentle trituration. After

300 rpm centrifugation for 10 min, the supernatant and cellular components were separated.

Transmission Electron Microscopy

Retinal samples were fixed with 2.5% glutaraldehyde and subjected to examination by transmission electron microscopy (TEM). Sections (1 μm thick) were stained with methylene blue and thin-sectioned with a diamond knife. The sections were collected on mesh grids, stained with uranyl acetate and lead citrate, and examined under an electron microscope (1230 EXII; JOEL).

Quantitative RT-PCR Analysis

Total RNA was prepared from retinal tissues and reverse transcription was performed using Superscript II (Invitrogen). Quantitative PCR assays were performed with an ABI 7500 Fast Real-Time PCR System using TaqMan Fast Universal PCR master mix (Applied Biosystems) and TaqMan Gene Expression assay mix of *vegfa* (Mm00437304_ml), *vegfc* (Mm01202432_ml), *vegfr2* (Mm00440099_ml), *vegfr1* (Mm00438780_ml), *angpt1* (Mm00456503_ml), *angpt2* (Mm00545822_ml), *tek* (Mm00443242_ml), *dll4* (Mm00444619_m1), *notch1* (Mm00435259_ml), *cxcl12* (Mm00445552_ml), *cxcr4* (Mm01292123_ml), *hif1a* (Mm00468878_ml), and *tgfb1* (Mm00441724_m1). A mouse β -actin (Mm00607939_s1) assay mix served as an endogenous control. Data were analyzed using 7500 Fast System SDS software 1.3.1. Each experiment was performed with four replicates from each sample, and the results were averaged.

Cell Culture

Retinal cell culture was performed according to a previous report (Kubota et al., 2011). Briefly, retinal tissues were incubated for 30 min at 37°C in DMEM containing 1% collagenase D (from *Clostridium histolyticum*) before cells were dissociated by gentle trituration. A flow cytometer, SORP FACS Aria (BD) with FlowJo software (TreeStar) was used to analyze stained samples. GFP⁺ cells were sorted from the P1 retinas of Pax6 α -Cre⁺/flox-CAT-EGFP⁺ mice using fluorescence-activated cell sorting (FACS). Cells were washed and resuspended in DMEM containing 10% fetal bovine serum and then plated on poly-D-lysine-coated culture slides. The samples were incubated at 37°C in 20% O₂. Cells were supplemented with recombinant hVEGF₁₆₅ proteins (Peprotech) labeled with Alexa Fluor 546 using a labeling kit (Molecular Probes) according to the manufacturers' instruction and a previous paper (Nakayama et al., 2013). Ten minutes after incubation with Alexa546-labeled hVEGF, the culture medium was replaced with medium free from Alexa546-labeled hVEGF.

Electroretinography

Electroretinography was performed as previously described (Kurihara et al., 2010). The responses were differentially amplified and filtered through a digital bandpass filter ranging from 0.313 to 1000 Hz to yield a- and b-waves. Light pulses of 800 cd \times s/m² and 4 ms duration were delivered via a commercial Ganzfeld stimulator (Ganzfeld System SG-2002; LKC Technologies). The amplitude of the a-wave was measured from the baseline to the trough of the a-wave, and the amplitude of the b-wave was determined from the trough of the a-wave to the peak of the b-wave. The implicit time of the a- and b-waves was measured from the onset of stimuli to the peak of each wave.

Statistical Analysis

Results are expressed as the mean \pm SD. The comparisons between the averages of the two groups were evaluated using the two-tailed Student's t test. The p values < 0.05 were considered statistically significant.

SUPPLEMENTAL INFORMATION

Supplemental Information includes six figures and can be found with this article online at <http://dx.doi.org/10.1016/j.cell.2014.09.025>.

AUTHOR CONTRIBUTIONS

K.O., S.K., T.Y., T.K., and I.T.-N. performed experiments. T.S. assisted in manuscript preparation. M.E., T.M., Y.M., and T.N.S. provided experimental

materials. Y.K. designed experiments, performed experiments, interpreted results, and wrote the paper.

ACKNOWLEDGMENTS

We thank Toshihiro Nagai and Naoko Numata (Keio University) for their technical supports, and Institute of Immunology (Utsunomiya, Japan) for helping us generate some of the mutant mice. This work was supported by Grants-in-Aid for Specially Promoted Research from the Ministry of Education, Culture, Sports, Science and Technology of Japan, by a research grant from Takeda Science Foundation, The Kanae Foundation, The Mochida Memorial Foundation, SENSHIN Medical Research Foundation, Daiichi Sankyo Foundation of Life Science, and The Naito Foundation.

Received: April 21, 2014

Revised: July 29, 2014

Accepted: September 10, 2014

Published: October 23, 2014

REFERENCES

- Adams, R.H., and Eichmann, A. (2010). Axon guidance molecules in vascular patterning. *Cold Spring Harb. Perspect. Biol.* 2, a001875.
- Albuquerque, R.J., Hayashi, T., Cho, W.G., Kleinman, M.E., Dridi, S., Takeda, A., Baffi, J.Z., Yamada, K., Kaneko, H., Green, M.G., et al. (2009). Alternatively spliced vascular endothelial growth factor receptor-2 is an essential endogenous inhibitor of lymphatic vessel growth. *Nat. Med.* 15, 1023–1030.
- Bellon, A., Luchino, J., Haigh, K., Rougon, G., Haigh, J., Chauvet, S., and Mann, F. (2010). VEGFR2 (KDR/Fik1) signaling mediates axon growth in response to semaphorin 3E in the developing brain. *Neuron* 66, 205–219.
- Binet, F., Mawambo, G., Sitaras, N., Tetreault, N., Lapalme, E., Favret, S., Cerani, A., Leboeuf, D., Tremblay, S., Rezende, F., et al. (2013). Neuronal ER stress impedes myeloid-cell-induced vascular regeneration through IRE1 α degradation of netrin-1. *Cell Metab.* 17, 353–371.
- de Boer, J., Williams, A., Skavdis, G., Harker, N., Coles, M., Tolaini, M., Norton, T., Williams, K., Roderick, K., Potocnik, A.J., and Kioussis, D. (2003). Transgenic mice with hematopoietic and lymphoid specific expression of Cre. *Eur. J. Immunol.* 33, 314–325.
- Dorrell, M.I., Aguilar, E., and Friedlander, M. (2002). Retinal vascular development is mediated by endothelial filopodia, a preexisting astrocytic template and specific R-cadherin adhesion. *Invest. Ophthalmol. Vis. Sci.* 43, 3500–3510.
- Dorrell, M.I., Aguilar, E., Jacobson, R., Yanes, O., Gariano, R., Heckenlively, J., Banin, E., Ramirez, G.A., Gasmi, M., Bird, A., et al. (2009). Antioxidant or neurotrophic factor treatment preserves function in a mouse model of neovascularization-associated oxidative stress. *J. Clin. Invest.* 119, 611–623.
- Ema, M., Yokomizo, T., Wakamatsu, A., Terunuma, T., Yamamoto, M., and Takahashi, S. (2006). Primitive erythropoiesis from mesodermal precursors expressing VE-cadherin, PECAM-1, Tie2, endoglin, and CD34 in the mouse embryo. *Blood* 108, 4018–4024.
- Erskine, L., Reijntjes, S., Pratt, T., Denti, L., Schwarz, Q., Vieira, J.M., Alakone, B., Shewan, D., and Ruhrberg, C. (2011). VEGF signaling through neuropilin 1 guides commissural axon crossing at the optic chiasm. *Neuron* 70, 951–965.
- Ferguson, S.M., Raimondi, A., Paradise, S., Shen, H., Mesaki, K., Ferguson, A., Destaing, O., Ko, G., Takasaki, J., Cremona, O., et al. (2009). Coordinated actions of actin and BAR proteins upstream of dynamin at endocytic clathrin-coated pits. *Dev. Cell* 17, 811–822.
- Fruttiger, M., Calver, A.R., Krüger, W.H., Mudhar, H.S., Michalovich, D., Takakura, N., Nishikawa, S., and Richardson, W.D. (1996). PDGF mediates a neuron-astrocyte interaction in the developing retina. *Neuron* 17, 1117–1131.

- Gariano, R.F., and Gardner, T.W. (2005). Retinal angiogenesis in development and disease. *Nature* 438, 960–966.
- Gerber, H.P., Hillan, K.J., Ryan, A.M., Kowalski, J., Keller, G.A., Rangell, L., Wright, B.D., Radtke, F., Aguet, M., and Ferrara, N. (1999). VEGF is required for growth and survival in neonatal mice. *Development* 126, 1149–1159.
- Gerhardt, H., Golding, M., Fruttiger, M., Ruhrberg, C., Lundkvist, A., Abramson, A., Jeltsch, M., Mitchell, C., Alitalo, K., Shima, D., and Betsholtz, C. (2003). VEGF guides angiogenic sprouting utilizing endothelial tip cell filopodia. *J. Cell Biol.* 161, 1163–1177.
- Haase, V.H., Glickman, J.N., Socolovsky, M., and Jaenisch, R. (2001). Vascular tumors in livers with targeted inactivation of the von Hippel-Lindau tumor suppressor. *Proc. Natl. Acad. Sci. USA* 98, 1583–1588.
- Haigh, J.J., Morelli, P.I., Gerhardt, H., Haigh, K., Tsien, J., Damert, A., Miquero, L., Muhlnner, U., Klein, R., Ferrara, N., et al. (2003). Cortical and retinal defects caused by dosage-dependent reductions in VEGF-A paracrine signaling. *Dev. Biol.* 262, 225–241.
- Hooper, A.T., Butler, J.M., Nolan, D.J., Kranz, A., Iida, K., Kobayashi, M., Kopp, H.G., Shido, K., Petit, I., Yanger, K., et al. (2009). Engraftment and reconstitution of hematopoiesis is dependent on VEGFR2-mediated regeneration of sinusoidal endothelial cells. *Cell Stem Cell* 4, 263–274.
- Ishitobi, H., Matsumoto, K., Azami, T., Itoh, F., Itoh, S., Takahashi, S., and Ema, M. (2010). Flk1-GFP BAC Tg mice: an animal model for the study of blood vessel development. *Exp. Anim.* 59, 615–622.
- Ishitobi, H., Wakamatsu, A., Liu, F., Azami, T., Hamada, M., Matsumoto, K., Kataoka, H., Kobayashi, M., Choi, K., Nishikawa, S., et al. (2011). Molecular basis for Flk1 expression in hemato-cardiovascular progenitors in the mouse. *Development* 138, 5357–5368.
- Kubo, F., Takeichi, M., and Nakagawa, S. (2005). Wnt2b inhibits differentiation of retinal progenitor cells in the absence of Notch activity by downregulating the expression of proneural genes. *Development* 132, 2759–2770.
- Kubota, Y., Takubo, K., Hirashima, M., Nagoshi, N., Kishi, K., Okuno, Y., Nakamura-Ishizu, A., Sano, K., Murakami, M., Ema, M., et al. (2011). Isolation and function of mouse tissue resident vascular precursors marked by myelin protein zero. *J. Exp. Med.* 208, 949–960.
- Kurihara, T., Kubota, Y., Ozawa, Y., Takubo, K., Noda, K., Simon, M.C., Johnson, R.S., Suematsu, M., Tsubota, K., Ishida, S., et al. (2010). von Hippel-Lindau protein regulates transition from the fetal to the adult circulatory system in retina. *Development* 137, 1563–1571.
- Lambrechts, D., Storkebaum, E., Morimoto, M., Del-Favero, J., Desmet, F., Marklund, S.L., Wyns, S., Thijs, V., Andersson, J., van Marion, I., et al. (2003). VEGF is a modifier of amyotrophic lateral sclerosis in mice and humans and protects motoneurons against ischemic death. *Nat. Genet.* 34, 383–394.
- Lampugnani, M.G., Orsenigo, F., Gagliani, M.C., Tacchetti, C., and Dejana, E. (2006). Vascular endothelial cadherin controls VEGFR-2 internalization and signaling from intracellular compartments. *J. Cell Biol.* 174, 593–604.
- Lang, R.A. (1997). Apoptosis in mammalian eye development: lens morphogenesis, vascular regression and immune privilege. *Cell Death Differ.* 4, 12–20.
- Lee, S., Chen, T.T., Barber, C.L., Jordan, M.C., Murdock, J., Desai, S., Ferrara, N., Nagy, A., Roos, K.P., and Iruela-Arispe, M.L. (2007). Autocrine VEGF signaling is required for vascular homeostasis. *Cell* 130, 691–703.
- Lillien, L., and Cepko, C. (1992). Control of proliferation in the retina: temporal changes in responsiveness to FGF and TGF alpha. *Development* 115, 253–266.
- Lu, X., Le Noble, F., Yuan, L., Jiang, Q., De Lafarge, B., Sugiyama, D., Bréant, C., Claes, F., De Smet, F., Thomas, J.L., et al. (2004). The netrin receptor UNC5B mediates guidance events controlling morphogenesis of the vascular system. *Nature* 432, 179–186.
- Luo, L., Uehara, H., Zhang, X., Das, S.K., Olsen, T., Holt, D., Simonis, J.M., Jackman, K., Singh, N., Miya, T.R., et al. (2013). Photoreceptor avascular privilege is shielded by soluble VEGF receptor-1. *eLife* 2, e00324.
- Marquardt, T., Ashery-Padan, R., Andrejewski, N., Scardigli, R., Guillemot, F., and Gruss, P. (2001). Pax6 is required for the multipotent state of retinal progenitor cells. *Cell* 105, 43–55.
- Matsumoto, K., Azami, T., Otsu, A., Takase, H., Ishitobi, H., Tanaka, J., Miwa, Y., Takahashi, S., and Ema, M. (2012). Study of normal and pathological blood vessel morphogenesis in Flt1-tdsRed BAC Tg mice. *Genesis* 50, 561–571.
- Milde, F., Lauw, S., Koumoutsakos, P., and Iruela-Arispe, M.L. (2013). The mouse retina in 3D: quantification of vascular growth and remodeling. *Integr. Biol. (Camb.)* 5, 1426–1438.
- Mohyeldin, A., Garzón-Muvdi, T., and Quiñones-Hinojosa, A. (2010). Oxygen in stem cell biology: a critical component of the stem cell niche. *Cell Stem Cell* 7, 150–161.
- Mukouyama, Y.S., Shin, D., Britsch, S., Taniguchi, M., and Anderson, D.J. (2002). Sensory nerves determine the pattern of arterial differentiation and blood vessel branching in the skin. *Cell* 109, 693–705.
- Nakamura-Ishizu, A., Kurihara, T., Okuno, Y., Ozawa, Y., Kishi, K., Goda, N., Tsubota, K., Okano, H., Suda, T., and Kubota, Y. (2012). The formation of an angiogenic astrocyte template is regulated by the neuroretina in a HIF-1-dependent manner. *Dev. Biol.* 363, 106–114.
- Nakayama, M., Nakayama, A., van Lessen, M., Yamamoto, H., Hoffmann, S., Drexler, H.C., Itoh, N., Hirose, T., Breier, G., Vestweber, D., et al. (2013). Spatial regulation of VEGF receptor endocytosis in angiogenesis. *Nat. Cell Biol.* 15, 249–260.
- Nishijima, K., Ng, Y.S., Zhong, L., Bradley, J., Schubert, W., Jo, N., Akita, J., Samuelsson, S.J., Robinson, G.S., Adamis, A.P., and Shima, D.T. (2007). Vascular endothelial growth factor-A is a survival factor for retinal neurons and a critical neuroprotectant during the adaptive response to ischemic injury. *Am. J. Pathol.* 171, 53–67.
- Pitulescu, M.E., Schmidt, I., Benedito, R., and Adams, R.H. (2010). Inducible gene targeting in the neonatal vasculature and analysis of retinal angiogenesis in mice. *Nat. Protoc.* 5, 1518–1534.
- Potente, M., Gerhardt, H., and Carmeliet, P. (2011). Basic and therapeutic aspects of angiogenesis. *Cell* 146, 873–887.
- Ruhrberg, C., Gerhardt, H., Golding, M., Watson, R., Ioannidou, S., Fujisawa, H., Betsholtz, C., and Shima, D.T. (2002). Spatially restricted patterning cues provided by heparin-binding VEGF-A control blood vessel branching morphogenesis. *Genes Dev.* 16, 2684–2698.
- Ryan, H.E., Poloni, M., McNulty, W., Elson, D., Gassmann, M., Arbeit, J.M., and Johnson, R.S. (2000). Hypoxia-inducible factor-1alpha is a positive factor in solid tumor growth. *Cancer Res.* 60, 4010–4015.
- Saint-Geniez, M., Maharaj, A.S., Walshe, T.E., Tucker, B.A., Sekiyama, E., Kurihara, T., Darland, D.C., Young, M.J., and D'Amore, P.A. (2008). Endogenous VEGF is required for visual function: evidence for a survival role on müller cells and photoreceptors. *PLoS ONE* 3, e3554.
- Sapieha, P., Sirinyan, M., Hamel, D., Zaniolo, K., Joyal, J.S., Cho, J.H., Honoré, J.C., Kermorvant-Duchemin, E., Varma, D.R., Tremblay, S., et al. (2008). The succinate receptor GPR91 in neurons has a major role in retinal angiogenesis. *Nat. Med.* 14, 1067–1076.
- Shalaby, F., Ho, J., Stanford, W.L., Fischer, K.D., Schuh, A.C., Schwartz, L., Bernstein, A., and Rossant, J. (1997). A requirement for Flk1 in primitive and definitive hematopoiesis and vasculogenesis. *Cell* 89, 981–990.
- Smith, L.E., Wesolowski, E., McLellan, A., Kostyk, S.K., D'Amato, R., Sullivan, R., and D'Amore, P.A. (1994). Oxygen-induced retinopathy in the mouse. *Invest. Ophthalmol. Vis. Sci.* 35, 101–111.
- Stefater, J.A., 3rd, Lewkowich, I., Rao, S., Mariggi, G., Carpenter, A.C., Burr, A.R., Fan, J., Ajima, R., Molkentin, J.D., Williams, B.O., et al. (2011). Regulation of angiogenesis by a non-canonical Wnt-Flt1 pathway in myeloid cells. *Nature* 474, 511–515.

- Stenzel, D., Lundkvist, A., Sauvaget, D., Busse, M., Graupera, M., van der Flier, A., Wijelath, E.S., Murray, J., Sobel, M., Costell, M., et al. (2011). Integrin-dependent and -independent functions of astrocytic fibronectin in retinal angiogenesis. *Development* *138*, 4451–4463.
- Wang, Y., Rattner, A., Zhou, Y., Williams, J., Smallwood, P.M., and Nathans, J. (2012). Norrin/Frizzled4 signaling in retinal vascular development and blood brain barrier plasticity. *Cell* *151*, 1332–1344.
- Yang, X., and Cepko, C.L. (1996). Flk-1, a receptor for vascular endothelial growth factor (VEGF), is expressed by retinal progenitor cells. *J. Neurosci.* *16*, 6089–6099.
- Ye, X., Wang, Y., Cahill, H., Yu, M., Badea, T.C., Smallwood, P.M., Peachey, N.S., and Nathans, J. (2009). Norrin, frizzled-4, and Lrp5 signaling in endothelial cells controls a genetic program for retinal vascularization. *Cell* *139*, 285–298.

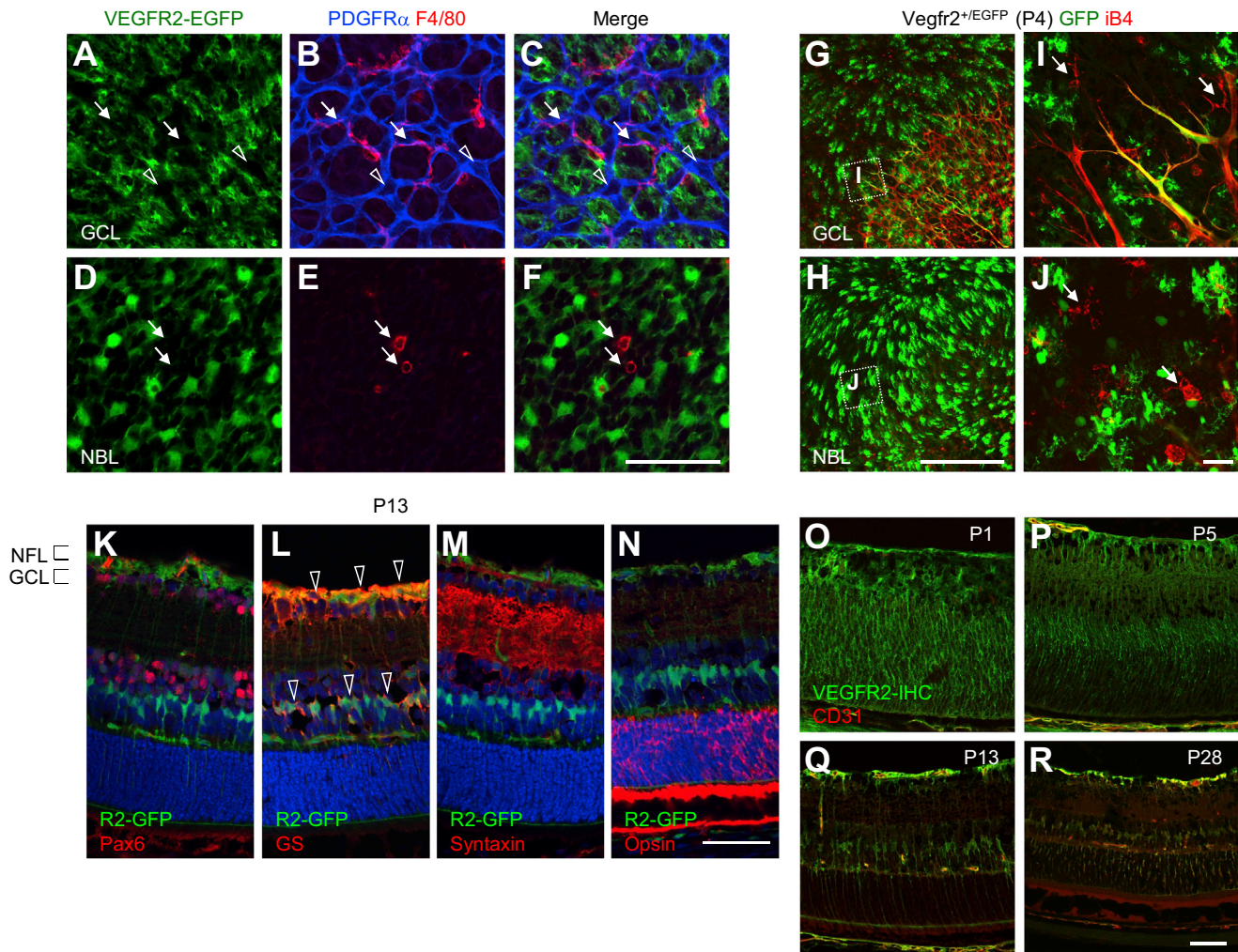


Figure S1. Expression Pattern of VEGFR2 in Developing Retina, Related to Figure 1

(A–F) Whole-mount staining of the retina from *Vegfr2-BAC-EGFP*⁺ mice at P6. GFP immunoreactivity is detected in neuroretinal cells of both the ganglion cell layer (GCL) and the neuroblastic layer (NBL), but not in PDGFR α ⁺ astrocytes (open arrowheads) and F4/80⁺ macrophages (arrows).

(G–J) Whole-mount staining of the retina from *Vegfr2*^{+/EGFP} mice at P6. Mosaic but strong immunoreactivity of GFP is detected in neuroretinal cells. PDGFR α ⁺ astrocytes and iB4⁺ macrophages do not show GFP positivity.

(K–N) Immunohistochemistry of retinal sections from *Vegfr2-BAC-EGFP*⁺ mice at P13. GFP positivity detected in glutamine synthase (GS)⁺ Muller cells (open arrowheads) but not in Pax6⁺ retinal progenitor cells, Syntaxin⁺ amacrine cells, and opsin⁺ photoreceptor cells.

(O–R) Immunohistochemistry of retinal sections at various stages. Scale bars: 500 μ m (G, H); 50 μ m (A–F, I–R).

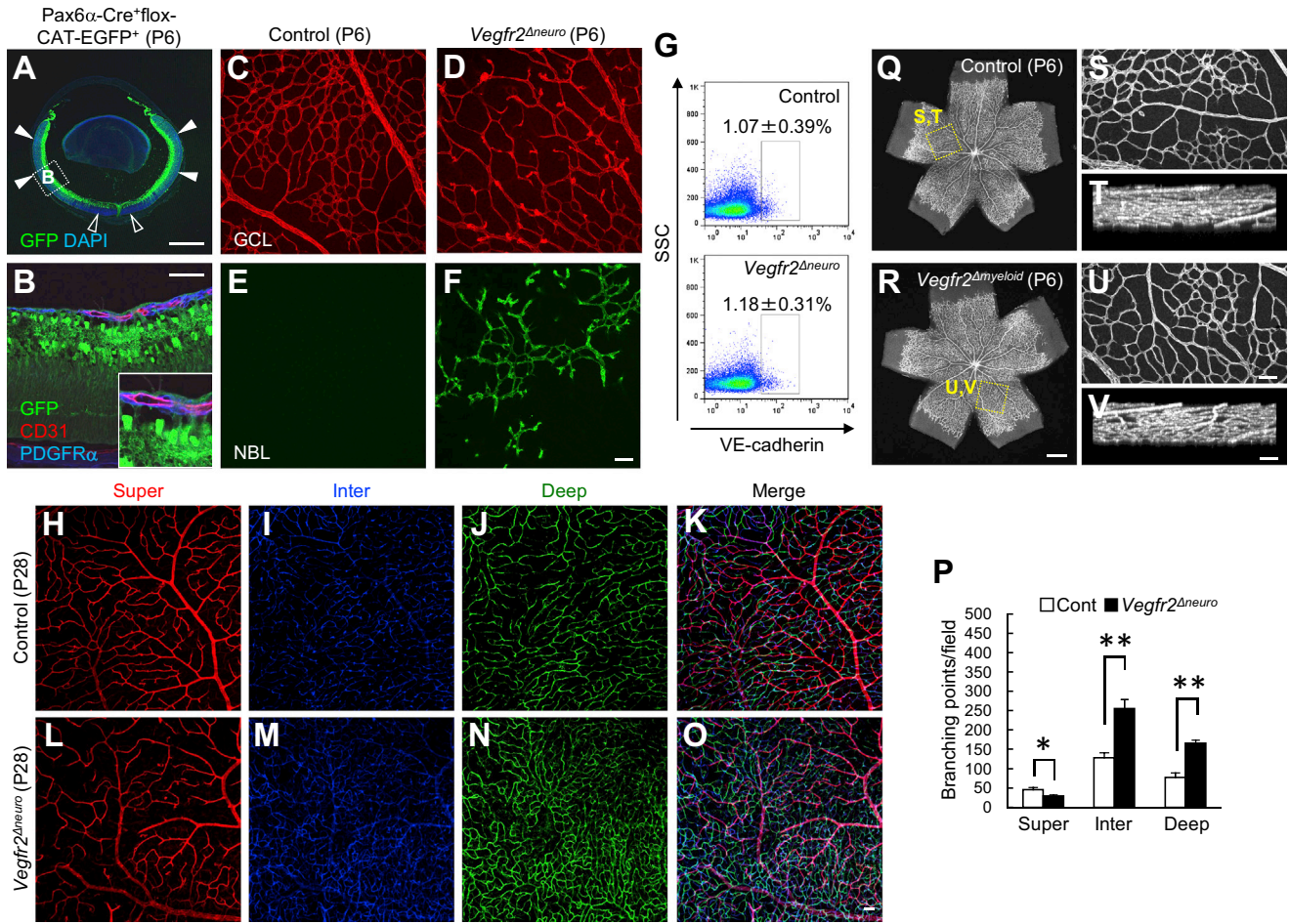


Figure S2. Misdirected Sprouting in Neuronal, but Not Myeloid, *Vegfr2* Knockout, Related to Figure 2
 (A and B) Immunohistochemistry of retinal sections from *Pax6α-Cre⁺flox-CAT-EGFP⁺* mice at P6. GFP⁺ cells are detected in neuroretinal cells throughout the retina (closed arrowheads), except for the central area near the optic nerve head (open arrowheads). Panel (B) shows a high magnification view of the area indicated by the dotted square in (A). PDGFRα⁺ astrocytes and CD31⁺ endothelial cells do not show GFP positivity.
 (C–F) Single slices of confocal images from the area shown in Figures 2B and 2F as 3-dimensional deconvolution images.
 (G) Fluorescence-activated cell sorting (FACS) analysis and quantification (n = 3) of VE-cadherin for retinal tissues at P6.
 (H–P) Whole-mount staining of retina at P28 and quantification (n = 4).
 (Q–V) Whole-mount staining of the retina at P6. *Vegfr2^{Δmyeloid}* indicates the retina of *Vav1-iCre⁺Vegfr2^{flox/flox}* mice. Scale bars: 500 μm (A), (Q), (R); 50 μm (B), C–F, H–O, S–V). *p < 0.05; **p < 0.01. Data are represented as mean ± SD.

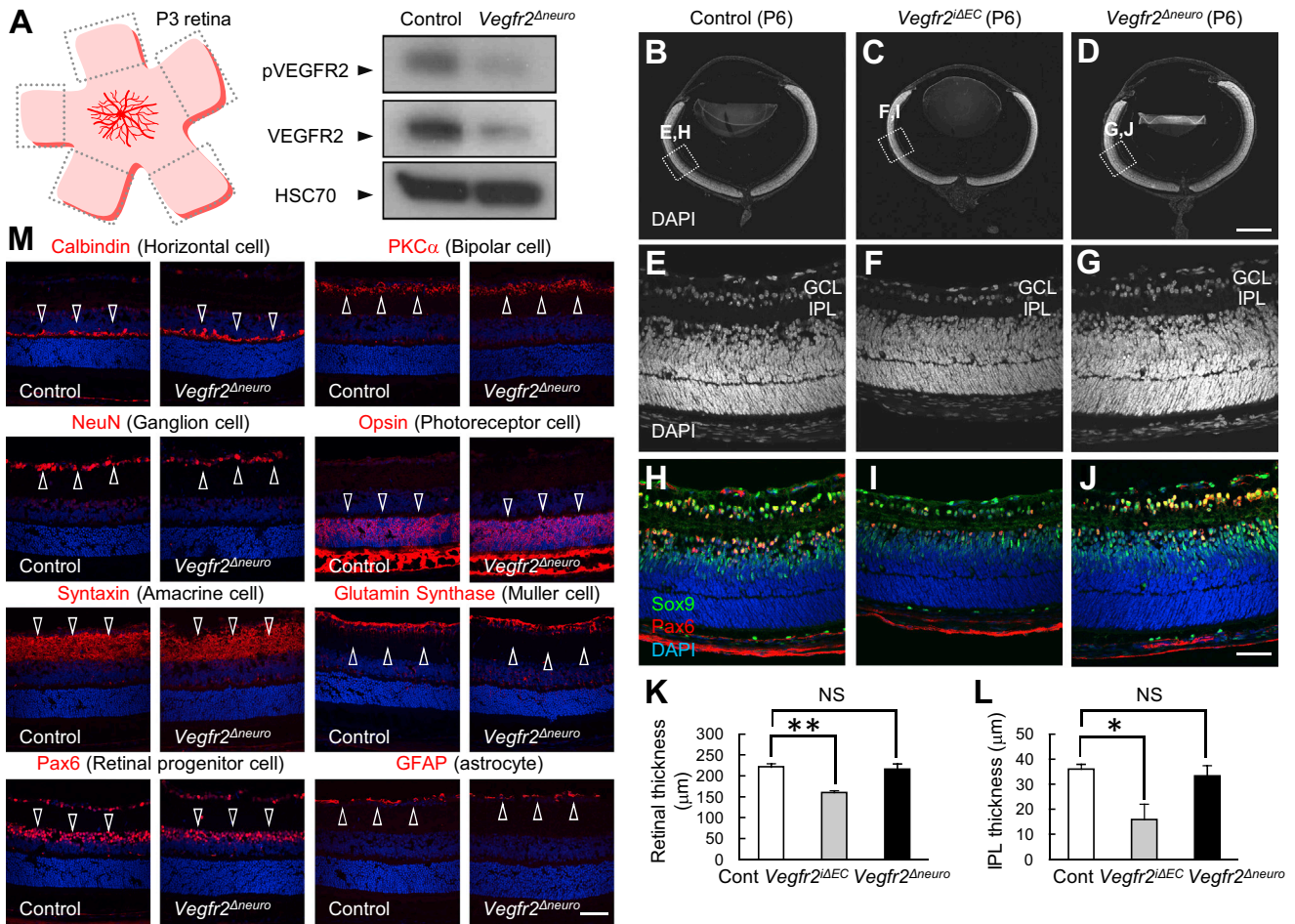


Figure S3. Neuroretinal Phenotypes in Neuronal *Vegfr2* Knockout, Related to Figure 3

(A) Immunoblot analysis on the peripheral half of retinal tissues at P3. Both phosphorylated VEGFR2 (pVEGFR2) and VEGFR2 proteins are markedly decreased in *Vegfr2^{Δneuro}* mice.

(B–L) Immunohistochemistry and quantification ($n = 4$) of retinal sections at P6. *Vegfr2^{ΔEC}* but not *Vegfr2^{Δneuro}* mice show decreased retinal thickness, particularly in the thickness of the inner plexiform layer (IPL) and the ganglion cell layer (GCL).

(M) Immunostaining with cell type-specific markers on 28 retinas. The differentiation into all neuronal cell types is completed in adult *Vegfr2^{Δneuro}* mice. Scale bars: 500 μm (B–D); 50 μm (E–J, M); * $p < 0.05$; ** $p < 0.01$; NS, not significant. Data are represented as mean \pm SD.

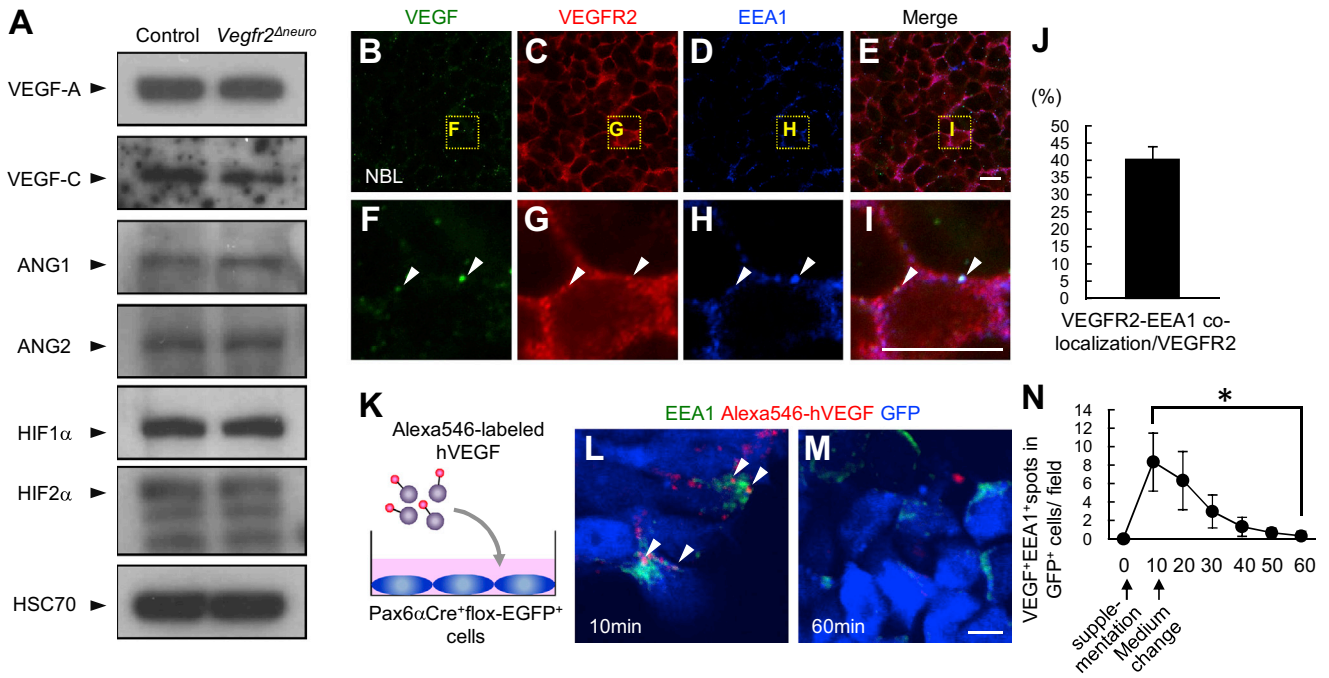
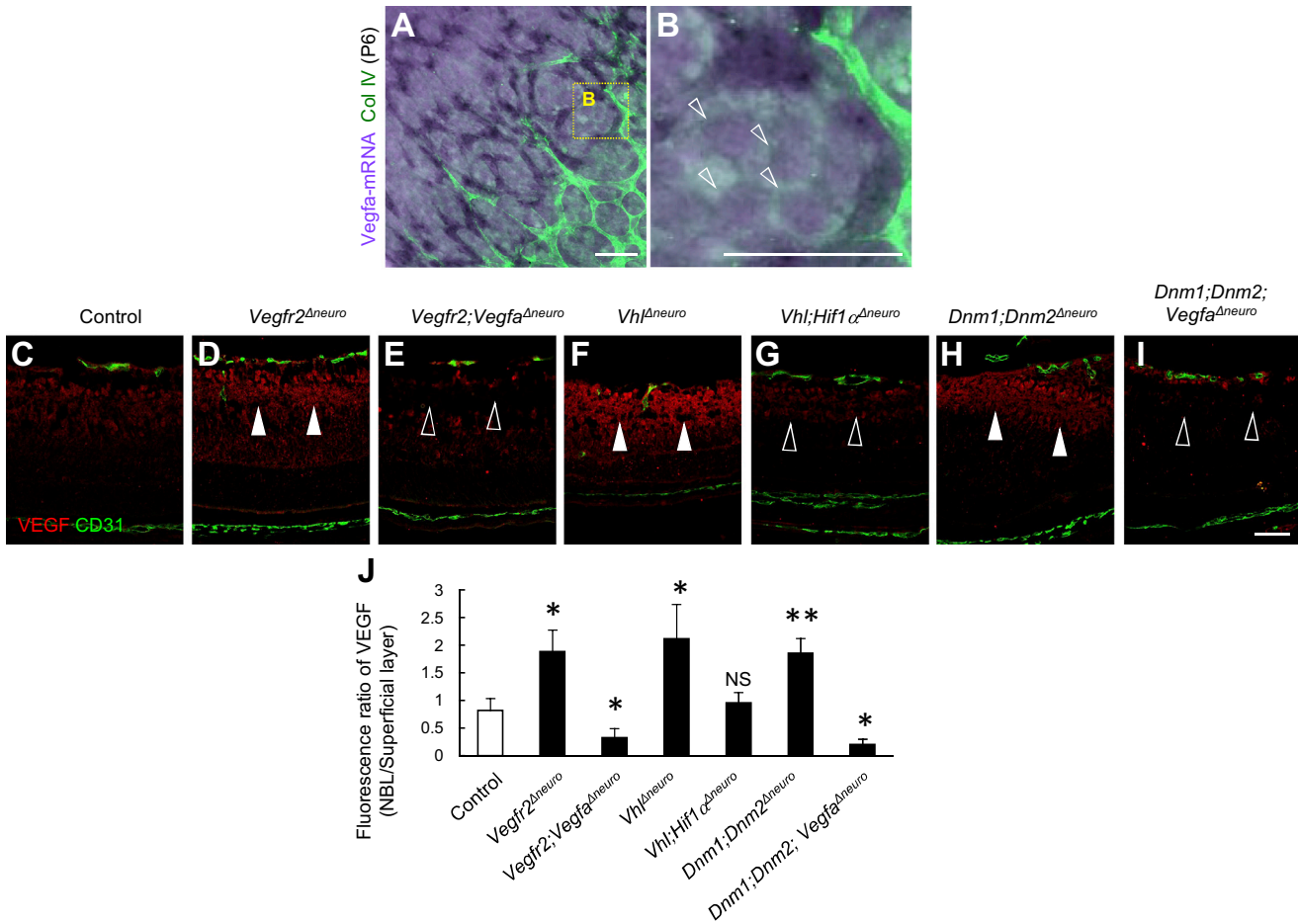


Figure S4. Tracking of Endocytosed VEGF, Related to Figure 4

(A) Immunoblot analysis on P3 retinal tissues.

(B–J) Immunohistochemistry and quantification (n = 4) of retinal whole-mounts at P6. Colocalization of endocytosed VEGF and VEGFR2 (arrowheads) is detected in retinal neurons.

(K–N) GFP⁺ cells are sorted from P1 retinas of *Pax6α-Cre⁺lox-EGFP⁺* mice using fluorescence-activated cell sorting (FACS). After 2 days of culture, cells are supplemented with recombinant hVEGF₁₆₅ proteins labeled with Alexa Fluor 546 for 10 min, and VEGF⁺EEA1⁺ spots in GFP⁺ cells (arrowheads) are quantified at each time point (n = 4). Scale bars: 10 μm; *p < 0.05. Data are represented as mean ± SD.



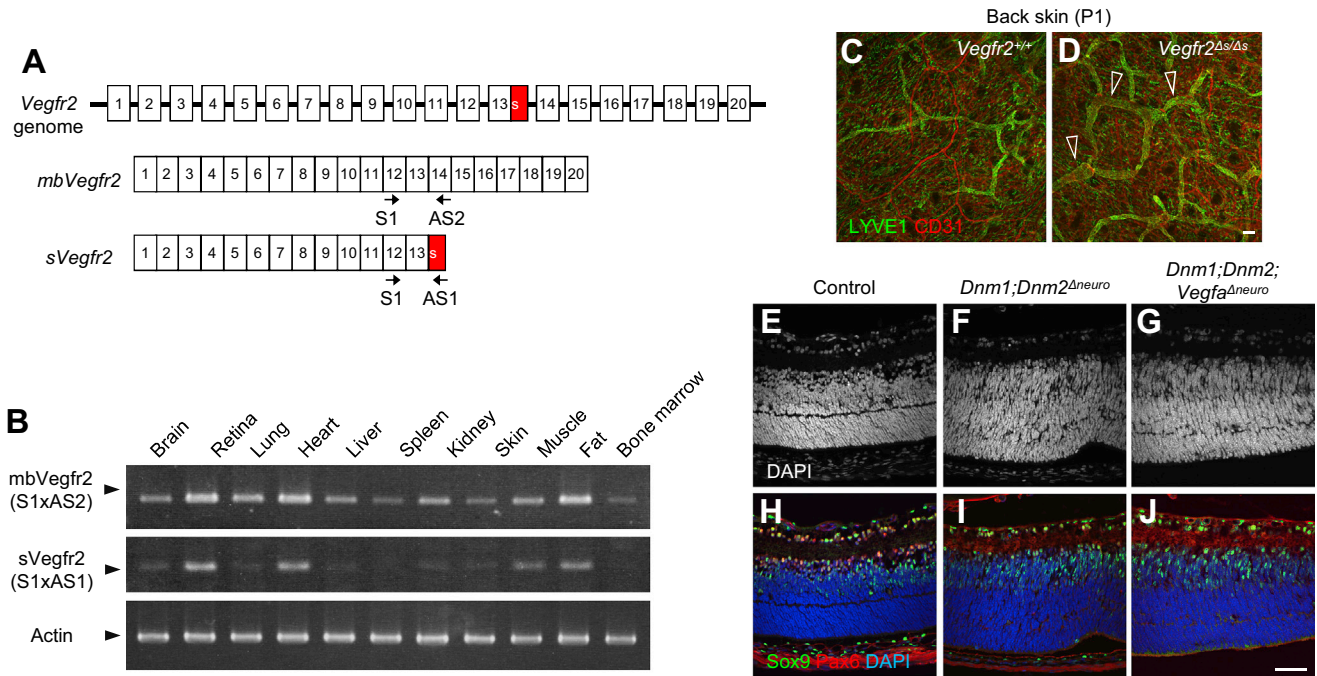


Figure S6. Expression and Function of sVegfr2, Related to Figure 6

(A) Scheme depicting splicing of the Vegfr2 gene and primer sets (S1: 5'-CGAGGAGAGAGGGTTCATCTC-3', AS1: 5'-CAGGGATGCCTCCATACC-3', AS2: 5'-GTCTGATTCTCCAGATTTCCG-3') designed to specifically detect mbVegfr2 and sVegfr2.

(B) RT-PCR analysis for various tissues at P5. sVegfr2 expression is relatively abundant in retina and heart.

(C and D) Whole-mount immunohistochemistry of P1 skins. Lymphatic vessels are apparently enlarged and hyperplastic (arrowheads) in sVEGFR2 knockout pups.

(E–J) Immunohistochemistry of retinal sections at P6. The morphology is largely normal, but insufficient separation of neuroblastic layers and reduced numbers of Pax6-positive cells are detected in Dnm1;Dnm2^{Δneuro} and Dnm1;Dnm2;Vegfa^{Δneuro} mice. Scale bar: 50 μm.